
CAMPA: Efficient and Aligned Multimodal Graph Learning via Decoupled Propagation and Aggregation

Daohan Su Hao Liu Xunkai Li Yinlin Zhu
 Xiong Yongfu Yi Liu Hongchao Qin Rong-Hua Li Guoren Wang

Abstract

Multimodal Graph Neural Networks (MGNNs) have shown strong potential for learning from multimodal attributed graphs, yet most existing approaches rely on tightly coupled architectures that suffer from prohibitive computational overhead. In this paper, we present a systematic empirical analysis showing that decoupled MGNNs are substantially more efficient and scalable for large-scale graph learning. However, we identify a critical bottleneck in existing decoupled pipelines, namely **modal conflict**, which arises in both the propagation and aggregation stages. Specifically, independent multi-hop diffusion causes cross-modal semantic divergence during propagation, while naive fusion fails to align multi-hop feature trajectories during aggregation, jointly limiting effective representation learning. To address this challenge, we propose **CAMPA**, a **C**ross-modal **A**ligned **M**ultimodal **P**ropagation & **A**ggregation framework for decoupled multimodal graph learning. Concretely, CAMPA introduces a two-stage alignment mechanism: (1) cross-modal aligned propagation, which injects cross-modal similarity priors into message passing to preserve semantic consistency without additional parameter overhead; (2) trajectory aligned aggregation, which leverages trajectory-level self-attention and cross-attention to capture and align long-range dependencies across modalities and hops. Extensive experiments on diverse benchmark datasets and tasks demonstrate that CAMPA consistently outperforms strong coupled and decoupled baselines while preserving the efficiency advantages of the decoupled paradigm.

1 Introduction

Learning on Multimodal Attributed Graphs (MAGs) has attracted growing attention as multimodal data and relational structures are increasingly intertwined in real-world systems, such as recommendation platforms and social media networks [12, 1, 43, 37, 29]. Meanwhile, graph neural networks (GNNs) have become a dominant paradigm for relational representation learning due to their strong ability to model high-order structural dependencies [19, 28, 5, 36, 42]. Unlike conventional GNNs that mainly operate on single-modality node attributes, multimodal GNNs (MGNNs) must jointly model heterogeneous semantic signals (e.g., text and images) together with graph topology, making effective multimodal fusion under structural constraints the central challenge in this domain [3, 21, 33].

A predominant paradigm in existing MGNNs relies on *coupled* architectures, where feature propagation and modality transformation are tightly intertwined within each layer [34, 27]. Although this design enables repeated topology-aware multimodal interaction, it also makes training expensive as graph size grows. This raises the first question: can the decoupling principle, which separates graph propagation from feature transformation and has been widely adopted for scalable graph learning [35, 9, 39], provide a more efficient foundation for MAG learning? To answer this question, we compare representative coupled baselines (i.e., MGAT [27] and MMGCN [34]) with decoupled baselines (e.g., MSGC, SIGN [9], and MGDN [17]) under the same MAG setting. As shown in Fig. 1(a), decoupled models reach comparable or better accuracy with substantially less training time, whereas coupled MGNNs incur much higher latency and quickly saturate. This observation

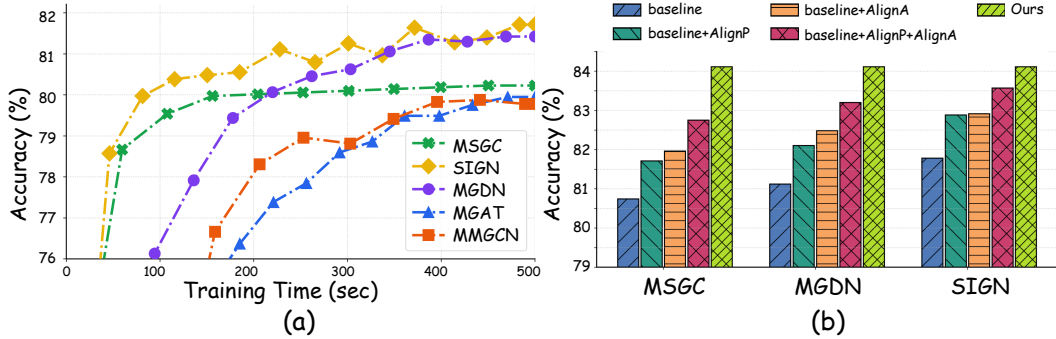


Figure 1: Empirical motivation. (a) Accuracy vs. training time, verifying the scalability advantage of decoupled architectures in MAG learning. (b) Performance boost of decoupled baselines after lightweight propagation-stage alignment (AlignP), aggregation-stage alignment (AlignA), or both, motivating explicit stage-wise coordination.

motivates decoupled architectures as a natural starting point for scalable multimodal graph learning, especially as recent MAG research moves toward larger graphs, more diverse objectives, stronger multimodal backbones, and graph-conditioned multimodal generation [7, 8, 24, 18, 29]. The complete experimental protocol is provided in Appendix A.1.

However, decoupling also raises a second question: what limitation emerges when multimodal interaction is weakened during the propagate-then-aggregate pipeline? In decoupled MAG models, modality-specific features are first diffused over the graph and then summarized by a lightweight fusion module. This pipeline can introduce modal conflict at two stages. (1) *Propagation stage*: text and image features originate from different semantic spaces, and independent multi-hop diffusion can make their hop-wise representations drift along modality-specific directions, producing spatial asynchrony. (2) *Aggregation stage*: after propagation, each modality forms a multi-hop trajectory, but naive late fusion struggles to match semantically corresponding hops across modalities, leading to trajectory-level mismatch. To examine whether these two stages are indeed bottlenecks, we equip representative decoupled baselines with lightweight propagation-stage and aggregation-stage alignment modules. Fig. 1(b) shows that both alignments improve decoupled baselines, and their combination yields the strongest gains. These intervention results motivate our central insight: scalable MAG learning requires not only decoupled computation, but also explicit stage-wise alignment during both propagation and aggregation. Additional heatmap and t-SNE visualizations in Appendix A.2 further illustrate the representation-level divergence behind this phenomenon.

Motivated by these critical insights, we propose **CAMPA** (**C**ross-modal **A**ligned **M**ultimodal **P**ropagation & **A**ggregation), a decoupled framework designed to resolve modal conflict while preserving the efficiency advantages of decoupled MGNNs. The key idea is to align multimodal information at the two stages where conflict arises. First, CAMPAs introduces *cross-modal aligned propagation*, which injects cross-modal similarity priors into the diffusion process to maintain semantic consistency during propagation without additional parameter overhead. Second, CAMPAs further employs *trajectory aligned aggregation*, which leverages trajectory-level self-attention and cross-attention to align multi-hop contextual dependencies across modalities during aggregation. In this way, CAMPAs strengthens cross-modal coordination while retaining the lightweight computation pattern that makes decoupled MGNNs attractive for large-scale learning.

Our contributions are summarized as follows: (1) *In-depth empirical insights*. We provide empirical evidence showing the scalability advantage of decoupled MGNNs and identify stage-wise modal conflict as a key bottleneck in both propagation and aggregation stages. (2) *A novel decoupled alignment framework*. We propose CAMPAs, a principled MAG learning framework that aligns multimodal information at both propagation and aggregation stages, thereby reconciling semantic alignment with the efficiency advantages of the decoupled paradigm. (3) *Strong performance across tasks*. Extensive experiments on diverse benchmark datasets and tasks demonstrate that CAMPAs consistently outperforms baselines while maintaining high efficiency.

2 Preliminaries

2.1 Problem Formulation

We consider a MAG $\mathcal{G} = (\mathcal{V}, \mathcal{E}, \{\mathbf{X}^{(m)}\}_{m \in \mathcal{M}})$, where \mathcal{V} and \mathcal{E} are the node and edge sets, \mathcal{M} is the modality index set, and $\mathbf{X}^{(m)} \in \mathbb{R}^{N \times d_m}$ is the feature matrix of modality m . The shared topology is represented by the adjacency matrix $\mathbf{A} \in \{0, 1\}^{N \times N}$ with degree matrix \mathbf{D} and normalized form $\tilde{\mathbf{A}} = \mathbf{D}^{-1/2} \mathbf{A} \mathbf{D}^{-1/2}$. For clarity, we instantiate the formulation on the common text-image setting, although it naturally extends to more modalities.

Following recent MAG studies and recent benchmark efforts [43, 37, 29], we consider two families of downstream tasks. **Graph-centric tasks** examine whether the learned node representations preserve both graph topology and multimodal semantics, including *Node Classification*, *Node Clustering*, and *Link Prediction*. **Modality-centric tasks** examine whether graph-aware representations improve cross-modal understanding and generation, including *Modality Retrieval*, *Modality Matching*, *Modality Alignment*, and *Graph-to-Image Generation* [38, 24, 8, 18].

2.2 Decoupled Graph Learning

Decoupled graph learning has become an important paradigm for scalable graph learning by explicitly separating structure propagation from feature transformation [35, 9, 4, 39]. Unlike coupled GNNs, which interleave neighborhood aggregation and parameterized transformation layer by layer, decoupled methods first compute multi-hop propagated features and then apply lightweight predictors on top. This separation substantially reduces training cost while preserving strong predictive performance on large graphs [40]. In a standard decoupled pipeline, the input feature matrix \mathbf{X} is transformed into a trajectory $\{\mathbf{H}^{(0)}, \mathbf{H}^{(1)}, \dots, \mathbf{H}^{(K)}\}$, where $\mathbf{H}^{(0)} = \mathbf{X}$ and $\mathbf{H}^{(k)}$ denotes the k -hop propagated representation. These trajectories are then aggregated by a learnable predictor, making decoupled graph learning attractive when propagation can be precomputed or reused across epochs.

2.3 Multimodal Attributed Graph Learning

MAG learning extends graph learning to MAGs by jointly modeling graph topology and modality attributes [43, 37, 29]. Existing MAG methods can be broadly summarized into three lines.

Conventional multimodal graph models typically adapt early multimodal recommendation architectures to graphs by designing topology-aware interaction or fusion modules [34, 27, 12]. These methods mainly emphasize topology-guided multimodal fusion and form the early foundation.

LLM- or token-based methods incorporate graph topology into multimodal reasoning through neighborhood tokenization, topology-aware aligners, or graph-conditioned generation modules [24, 8, 7, 18, 21, 33]. This line connects MAG learning with multimodal comprehension and generation by transforming structural information into tokenized contexts or auxiliary semantic priors.

Graph-enhanced methods further design specialized architectures, such as refined message passing, graph transformers, spectral filtering, or unified embedding spaces, to better capture topology-modality interplay [16, 15, 41, 13, 3, 20]. Compared with the previous two lines, these methods place greater emphasis on graph backbones and more expressive topology-aware multimodal interaction.

3 Method

We instantiate CAMPA on the common text-image setting, while the formulation naturally extends to more modalities. The raw inputs consist of graph topology together with node-associated textual and visual contents. Before graph learning, the text and image contents are encoded by a frozen pre-trained vision-language encoder, producing modality features that serve as the input of CAMPA. If the encoded modalities have different dimensionalities, lightweight modality-specific projections are further applied; for simplicity, we denote the resulting graph features as $\mathbf{H}_t^{(0)}, \mathbf{H}_i^{(0)} \in \mathbb{R}^{N \times d}$. As illustrated in Fig. 2, CAMPA follows a decoupled yet alignment-aware pipeline with two coordinated alignment components: **Cross-modal Aligned Propagation (CAP)** injects cross-modal semantic priors into graph diffusion, and **Trajectory Aligned Aggregation (TAA)** performs trajectory-level interaction and consistency-aware fusion over the propagated features.

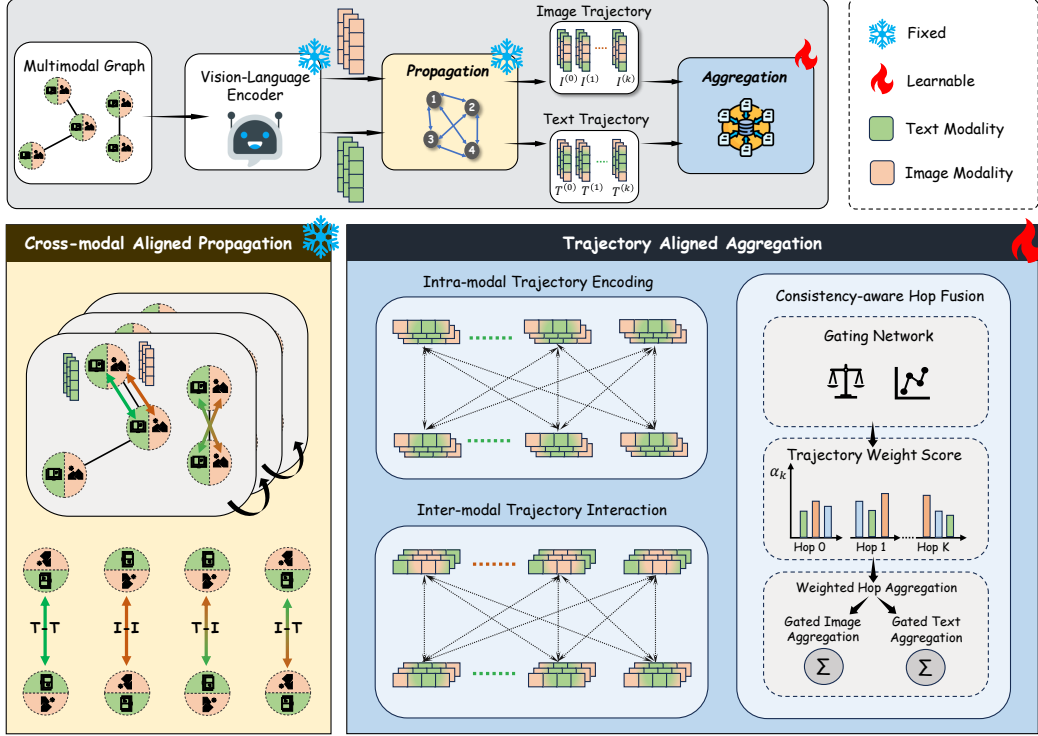


Figure 2: Overall framework of CAMPA. It first performs *cross-modal aligned propagation* to construct modality-specific multi-hop trajectories with cross-modal semantic priors injected into graph diffusion. It then applies *trajectory aligned aggregation* to model intra-modal hop dependencies and inter-modal trajectory interactions, producing unified node representations for downstream tasks.

3.1 Cross-modal Aligned Propagation

Existing decoupled MAG models typically diffuse each modality independently on the shared graph. While efficient, such a design ignores whether connected nodes are semantically compatible across modalities, causing the propagated trajectories to drift apart as the hop depth increases. CAP addresses this issue by refining the propagation operators with modality-aware semantic priors, while preserving the precomputable nature of decoupled diffusion.

Semantic Propagation Priors. For each modality pair $(u, v) \in \{t, i\} \times \{t, i\}$, we estimate edge-wise semantic priors from the initial node features and use them to modulate the shared topology:

$$\mathbf{S}_{uv} = \left(1 + \cos\text{-sim}\left(\mathbf{H}_u^{(0)}, \mathbf{H}_v^{(0)}\right)\right) / 2, \quad \tilde{\mathbf{A}}_{uv} = \text{Norm}(\mathbf{A} \odot \mathbf{S}_{uv}), \quad (1)$$

where the rescaling maps cosine similarity to $[0, 1]$, $\text{Norm}(\mathbf{B}) = \mathbf{D}_B^{-1/2} \mathbf{B} \mathbf{D}_B^{-1/2}$ is symmetric normalization, and \odot denotes the Hadamard product. Here, $\tilde{\mathbf{A}}_{tt}$ and $\tilde{\mathbf{A}}_{ii}$ preserve modality-specific local smoothness, whereas $\tilde{\mathbf{A}}_{ti}$ and $\tilde{\mathbf{A}}_{it}$ inject cross-modal correspondence into graph diffusion.

Aligned Multi-hop Diffusion. Let \bar{u} denote the counterpart modality of u . For each $u \in \{t, i\}$, CAP updates the k -hop representation by combining intra-modal diffusion, cross-modal correction, and residual retention:

$$\mathbf{H}_u^{(k+1)} = \alpha_u \tilde{\mathbf{A}}_{uu} \mathbf{H}_u^{(k)} + \beta_u \tilde{\mathbf{A}}_{u\bar{u}} \mathbf{H}_{\bar{u}}^{(k)} + \gamma_u \mathbf{H}_u^{(0)}, \quad \alpha_u + \beta_u + \gamma_u = 1, \quad (2)$$

where $\alpha_u, \beta_u, \gamma_u \geq 0$ are tunable hyperparameters. The first term captures modality-specific structural homophily, the second term continuously corrects the trajectory with aligned evidence from the other modality, and the residual branch stabilizes deep propagation. After K steps, we obtain two aligned propagation trajectories, $\{\mathbf{H}_t^{(0)}, \dots, \mathbf{H}_t^{(K)}\}$ and $\{\mathbf{H}_i^{(0)}, \dots, \mathbf{H}_i^{(K)}\}$. Notably, CAP introduces no hop-specific transformation during propagation, and thus remains fully compatible with the efficiency advantages of decoupled MAG learning.

3.2 Trajectory Aligned Aggregation

CAP produces alignment-aware multi-hop trajectories, yet directly averaging or concatenating them still overlooks two key aspects: different hops within one modality often play complementary roles, and cross-modal semantic agreement may emerge at different propagation depths. To address this, TAA models both intra-modal trajectory dependency and inter-modal trajectory interaction before performing adaptive hop fusion.

Intra-modal Trajectory Encoding. For each modality $u \in \{t, i\}$, we slightly abuse notation and stack the hop-wise propagated features as $\mathbf{H}_u = [\mathbf{H}_u^{(0)}, \dots, \mathbf{H}_u^{(K)}] \in \mathbb{R}^{N \times (K+1) \times d}$. All subsequent attention operations are applied along the trajectory dimension, while the node dimension is omitted as an implicit batch dimension. TAA first applies self-attention to capture dependencies among shallow and deep propagated features within the same modality:

$$\mathbf{Q}_u = \mathbf{H}_u \mathbf{W}_Q^u, \quad \mathbf{K}_u = \mathbf{H}_u \mathbf{W}_K^u, \quad \mathbf{V}_u = \mathbf{H}_u \mathbf{W}_V^u, \quad (3)$$

$$\mathbf{F}_u = \mathbf{H}_u + \text{MLP} \left(\text{softmax} \left(\frac{\mathbf{Q}_u \mathbf{K}_u^\top}{\sqrt{d}} \right) \mathbf{V}_u \right), \quad (4)$$

where $\mathbf{W}_Q^u, \mathbf{W}_K^u, \mathbf{W}_V^u \in \mathbb{R}^{d \times d}$ are learnable projections. This step contextualizes each hop with information from the entire propagation trajectory rather than treating different diffusion depths independently.

Inter-modal Trajectory Interaction. Based on the self-contextualized trajectories, we further introduce cross-attention to exchange complementary semantics across modalities:

$$\hat{\mathbf{Q}}_{u \leftarrow \bar{u}} = \mathbf{F}_u \mathbf{W}_Q^{u \leftarrow \bar{u}}, \quad \hat{\mathbf{K}}_{u \leftarrow \bar{u}} = \mathbf{F}_{\bar{u}} \mathbf{W}_K^{u \leftarrow \bar{u}}, \quad \hat{\mathbf{V}}_{u \leftarrow \bar{u}} = \mathbf{F}_{\bar{u}} \mathbf{W}_V^{u \leftarrow \bar{u}}, \quad (5)$$

$$\mathbf{G}_u = \mathbf{F}_u + \text{MLP} \left(\text{softmax} \left(\frac{\hat{\mathbf{Q}}_{u \leftarrow \bar{u}} \hat{\mathbf{K}}_{u \leftarrow \bar{u}}^\top}{\sqrt{d}} \right) \hat{\mathbf{V}}_{u \leftarrow \bar{u}} \right), \quad (6)$$

where $\mathbf{W}_Q^{u \leftarrow \bar{u}}, \mathbf{W}_K^{u \leftarrow \bar{u}}, \mathbf{W}_V^{u \leftarrow \bar{u}} \in \mathbb{R}^{d \times d}$. Unlike post-hoc late fusion, Eq. (6) aligns the two modalities at the trajectory level, enabling each hop to retrieve semantically compatible evidence from the other modality.

Consistency-aware Hop Fusion. After trajectory interaction, we estimate hop-wise cross-modal consistency and use it as an auxiliary signal for modality-specific hop weighting:

$$\mathbf{C} = \text{Cos}(\mathbf{G}_t, \mathbf{G}_i) \in \mathbb{R}^{N \times (K+1) \times 1}, \quad (7)$$

where $\text{Cos}(\cdot, \cdot)$ computes cosine similarity along the feature dimension for aligned hop slices. The hop weights of the two modalities are then predicted by separate gating networks:

$$\mathbf{A}_u = \text{Softmax}_{\text{hop}}(\mathcal{G}_u([\mathbf{G}_u \|\mathbf{C}])), \quad u \in \{t, i\}, \quad (8)$$

where $\mathcal{G}_t(\cdot)$ and $\mathcal{G}_i(\cdot)$ are modality-specific scoring networks, $\text{Softmax}_{\text{hop}}(\cdot)$ normalizes the scores along the hop dimension, and $\mathbf{A}_u^{(k)} \in \mathbb{R}^{N \times 1}$ denotes the hop weight for the k -th slice of modality u . The final representations are obtained by weighted aggregation over the aligned trajectories:

$$\mathbf{Z}_u = \sum_{k=0}^K \mathbf{A}_u^{(k)} \odot \mathbf{G}_u^{(k)}, \quad u \in \{t, i\}, \quad (9)$$

and the final representation for downstream prediction is formed as $\mathbf{Z} = \mathbf{Z}_t \|\mathbf{Z}_i$. This design preserves modality-specific aggregation preferences while still allowing the shared consistency signal to calibrate both gating processes.

3.3 Theoretical Analysis

We next formalize CAMPA from the perspectives of propagation stability and fusion control, with full proofs deferred to Appendix B.

3.3.1 Stable aligned diffusion in CAP

Let

$$\mathbf{X}^{(k)} = \begin{bmatrix} \mathbf{H}_t^{(k)} \\ \mathbf{H}_i^{(k)} \end{bmatrix}, \quad \mathbf{P} = \begin{bmatrix} \alpha_t \tilde{\mathbf{A}}_{tt} & \beta_t \tilde{\mathbf{A}}_{ti} \\ \beta_i \tilde{\mathbf{A}}_{it} & \alpha_i \tilde{\mathbf{A}}_{ii} \end{bmatrix}, \quad \mathbf{R} = \begin{bmatrix} \gamma_t \mathbf{I} & \mathbf{0} \\ \mathbf{0} & \gamma_i \mathbf{I} \end{bmatrix}. \quad (10)$$

Then Eq. (2) can be written as

$$\mathbf{X}^{(k+1)} = \mathbf{P}\mathbf{X}^{(k)} + \mathbf{R}\mathbf{X}^{(0)}. \quad (11)$$

Since each $\tilde{\mathbf{A}}_{uv}$ is symmetrically normalized, $\|\tilde{\mathbf{A}}_{uv}\|_2 \leq 1$. Define $\|\mathbf{X}\|_{2,\infty} = \max(\|\mathbf{X}_t\|_F, \|\mathbf{X}_i\|_F)$ for $\mathbf{X} = [\mathbf{X}_t; \mathbf{X}_i]$ and let $\rho = \max(\alpha_t + \beta_t, \alpha_i + \beta_i)$. Because $\alpha_u + \beta_u + \gamma_u = 1$, the condition $\rho < 1$ is naturally satisfied whenever $\gamma_t > 0$ and $\gamma_i > 0$.

Theorem 3.1 (Convergence and stability of CAP). *If $\rho < 1$, the CAP recursion in Eq. (11) admits the unique fixed point*

$$\mathbf{X}^* = (\mathbf{I} - \mathbf{P})^{-1} \mathbf{R}\mathbf{X}^{(0)}, \quad (12)$$

and its iterates satisfy

$$\|\mathbf{X}^{(k+1)} - \mathbf{X}^*\|_{2,\infty} \leq \rho \|\mathbf{X}^{(k)} - \mathbf{X}^*\|_{2,\infty}. \quad (13)$$

Theorem 3.1 shows that CAP preserves the stability of decoupled propagation after introducing cross-modal correction, while the residual branch prevents unbounded drift.

3.3.2 Discrepancy-controlled fusion in TAA

We next analyze the final hop fusion induced by TAA. For notational simplicity, we state the result for one node; since Eq. (9) is applied row-wise, the same conclusion holds independently for every node. Let $\mathbf{g}_u^{(k)} \in \mathbb{R}^d$ denote the k -th hop slice of modality u after trajectory interaction, and let $a_u^{(k)}$ be the corresponding hop weight produced by Eq. (8). Then Eq. (9) becomes

$$\mathbf{z}_u = \sum_{k=0}^K a_u^{(k)} \mathbf{g}_u^{(k)}, \quad u \in \{t, i\}, \quad (14)$$

where $a_u^{(k)} \geq 0$ and $\sum_{k=0}^K a_u^{(k)} = 1$ because the weights are normalized by softmax.

Proposition 3.2 (Bounded and discrepancy-controlled fusion). *For each modality $u \in \{t, i\}$, the fused representation \mathbf{z}_u is a convex combination of $\{\mathbf{g}_u^{(0)}, \dots, \mathbf{g}_u^{(K)}\}$. Moreover, the cross-modal discrepancy after hop fusion obeys*

$$\|\mathbf{z}_t - \mathbf{z}_i\|_2 \leq \sum_{k=0}^K a_t^{(k)} \|\mathbf{g}_t^{(k)} - \mathbf{g}_i^{(k)}\|_2 + \sum_{k=0}^K |a_t^{(k)} - a_i^{(k)}| \|\mathbf{g}_i^{(k)}\|_2. \quad (15)$$

The same bound also holds after swapping the roles of t and i .

Proposition 3.2 clarifies the role of TAA. The first term in Eq. (15) captures the residual hop-wise mismatch after trajectory interaction, while the second term reflects the discrepancy between the two modality-specific gating distributions. Accordingly, TAA improves fusion by jointly reducing trajectory mismatch and calibrating hop selection with the shared consistency signal. Appendix C further summarizes the end-to-end training procedure and computational complexity of CAMPAs.

4 Experiments

We design the experiments to answer the following questions: (Q1) Can CAMPAs consistently improve graph-centric prediction quality over both coupled and decoupled baselines? (Q2) Can the learned graph-aware multimodal representations also benefit modality-centric understanding tasks? (Q3) Which components in CAMPAs contribute most to the final gains? (Q4) Does CAMPAs preserve the efficiency advantages of decoupled MAG learning? (Q5) How sensitive is CAMPAs to the propagation depth and alignment rate?

Table 1: Performance comparison on representative graph-centric tasks. The best and second-best results are highlighted in **bold** and underline, respectively.

Tasks		Node Classification				Link Prediction		Node Clustering	
Methods	Goodreads		Grocery		Cloth		Movies		
	Acc	F1	Acc	F1	MRR	Hits@3	NMI	ARI	
GAT	58.94 \pm 0.23	53.02 \pm 0.18	81.01 \pm 0.21	72.94 \pm 0.24	42.89 \pm 0.25	51.05 \pm 0.28	40.21 \pm 0.28	31.48 \pm 0.33	
MMGCN	60.11 \pm 0.22	54.56 \pm 0.24	81.44 \pm 0.24	73.46 \pm 0.19	44.11 \pm 0.23	52.13 \pm 0.26	44.15 \pm 0.39	34.02 \pm 0.30	
MGAT	62.11 \pm 0.20	55.82 \pm 0.22	83.10 \pm 0.22	75.21 \pm 0.25	45.41 \pm 0.30	54.37 \pm 0.24	46.15 \pm 0.36	37.81 \pm 0.40	
SIGN	68.44 \pm 0.23	65.03 \pm 0.22	82.97 \pm 0.21	74.33 \pm 0.23	53.37 \pm 0.20	62.89 \pm 0.22	52.07 \pm 0.21	44.93 \pm 0.22	
MSGC	64.35 \pm 0.19	61.47 \pm 0.21	81.96 \pm 0.22	73.98 \pm 0.22	51.01 \pm 0.23	59.82 \pm 0.27	49.72 \pm 0.22	41.50 \pm 0.22	
MGDN	67.52 \pm 0.22	64.46 \pm 0.22	82.41 \pm 0.22	74.02 \pm 0.22	53.16 \pm 0.22	61.74 \pm 0.22	51.44 \pm 0.22	44.13 \pm 0.22	
DMGC	65.18 \pm 0.21	62.86 \pm 0.23	81.35 \pm 0.23	71.31 \pm 0.18	53.21 \pm 0.22	61.98 \pm 0.25	51.39 \pm 0.37	44.31 \pm 0.28	
DGF	70.21 \pm 0.19	64.05 \pm 0.22	83.31 \pm 0.22	74.01 \pm 0.24	53.19 \pm 0.29	62.21 \pm 0.23	52.18 \pm 0.34	45.01 \pm 0.39	
MIG-GT	70.16 \pm 0.25	66.35 \pm 0.20	82.46 \pm 0.20	74.43 \pm 0.22	57.14 \pm 0.27	64.93 \pm 0.30	47.31 \pm 0.31	39.71 \pm 0.36	
LGMRec	69.54 \pm 0.23	64.99 \pm 0.18	80.41 \pm 0.18	73.05 \pm 0.21	59.25 \pm 0.25	48.31 \pm 0.28	52.01 \pm 0.28	44.48 \pm 0.33	
UniGraph2	74.31 \pm 0.22	67.43 \pm 0.24	80.23 \pm 0.24	71.98 \pm 0.19	57.43 \pm 0.23	65.17 \pm 0.26	51.83 \pm 0.39	46.92 \pm 0.30	
CAMPA	76.93 \pm 0.20	67.29 \pm 0.22	84.98 \pm 0.21	81.01 \pm 0.23	60.33 \pm 0.30	68.17 \pm 0.24	56.53 \pm 0.36	48.93 \pm 0.40	

4.1 Experimental Setup

Datasets. We evaluate CAMPA on a diverse collection of MAG datasets spanning recommendation, social, and content understanding scenarios. Our experiments cover eight datasets, namely *Ele-fashion*, *Bili_music*, *RedditS*, *Movies*, *Goodreads*, *Grocery*, *Cloth*, and *SemArt*, following recent MAG benchmark protocols [22, 43, 37]. Detailed statistics are provided in Appendix D.

Baselines. We compare CAMPA with four groups of representative baselines. (1) *General graph baseline* includes GAT [28]. (2) *Early multimodal graph baselines* include MMGCN [34] and MGAT [27]. (3) *Recent strong multimodal baselines* include DMGC [11], DGF [41], MIG-GT [16], LGMRec [12], and UniGraph2 [13]. (4) *Decoupled baselines* include SIGN [9], MSGC [35], and MGDN [17], where MSGC denotes our multimodal adaptation of the classic SGC-style decoupled pipeline. Detailed descriptions of the compared baselines are provided in Appendix E.

Evaluation Protocol. We follow standard task-specific protocols in recent MAG studies and report both graph-centric and modality-centric metrics accordingly. All methods use the same data split and modality inputs on each dataset, while the detailed metric definitions, environment configuration, and hyperparameter settings are deferred to Appendices F and G.

4.2 Main Results

To answer **Q1** and **Q2**, we report representative results in the main text and defer broader benchmark tables to Appendix H. The two main tables jointly cover all eight datasets in our experiments.

Graph-centric tasks. We first examine whether CAMPA improves graph-aware representations on graph-centric benchmarks. These tasks directly test whether the learned embeddings preserve both structural signals and multimodal semantics. Table 1 shows that CAMPA achieves the strongest overall performance across the selected settings. For node classification, CAMPA attains the best accuracy on both *Goodreads* and *Grocery*, while also delivering the best F1 on *Grocery* and competitive F1 on *Goodreads*. For link prediction on *Cloth*, CAMPA improves the best previous MRR from 59.25 to 60.33 and the best previous Hits@3 from 65.17 to 68.17. For node clustering on *Movies*, CAMPA achieves the highest NMI and ARI, indicating that aligned propagation and trajectory-aware aggregation produce more coherent latent structures.

Modality-centric tasks. Beyond graph-centric prediction, we further investigate whether the graph-aware multimodal representations learned by CAMPA can benefit downstream cross-modal understanding. These tasks directly reflect whether the learned node representations are semantically coordinated across modalities rather than optimized only for structural prediction. Table 2 shows that the benefits of CAMPA extend beyond graph-centric benchmarks. For retrieval, CAMPA remains highly competitive on *Ele-fashion* and achieves the best T2I-MRR on *RedditS*, indicating that the learned graph-aware embeddings preserve strong bidirectional cross-modal correspondence. For graph-to-image generation, CAMPA achieves the best CLIP score on both *Bili_music* and *SemArt*, while also obtaining the best DINOv2 score on *SemArt*. These results together show that CAMPA improves not only graph prediction but also modality-level understanding and generation quality.

Table 2: Performance comparison on representative modality-centric tasks.

Tasks		Modality Retrieval				G2Image			
Methods	Ele-fashion		RedditS		Bili_music		SemArt		
	T2I-MRR	I2T-MRR	T2I-MRR	I2T-MRR	CLIP	DINOv2	CLIP	DINOv2	
GAT	96.82 \pm 0.10	96.50 \pm 0.13	77.51 \pm 0.15	77.23 \pm 0.10	49.42 \pm 0.16	21.00 \pm 0.19	53.21 \pm 0.14	39.46 \pm 0.15	
MMGCN	97.16 \pm 0.16	97.42 \pm 0.11	83.69 \pm 0.14	83.94 \pm 0.16	49.33 \pm 0.24	16.37 \pm 0.17	57.51 \pm 0.10	42.38 \pm 0.18	
MGAT	98.35 \pm 0.15	98.81 \pm 0.17	85.58 \pm 0.12	85.76 \pm 0.15	49.56 \pm 0.21	19.36 \pm 0.25	58.31 \pm 0.14	43.51 \pm 0.19	
SIGN	98.41 \pm 0.16	99.21 \pm 0.15	97.42 \pm 0.20	98.12 \pm 0.13	51.12 \pm 0.14	22.38 \pm 0.23	62.36 \pm 0.11	47.33 \pm 0.17	
MSGC	97.32 \pm 0.13	97.74 \pm 0.17	92.42 \pm 0.15	92.33 \pm 0.20	49.35 \pm 0.21	20.14 \pm 0.10	59.87 \pm 0.15	46.15 \pm 0.17	
MGDN	98.92 \pm 0.13	99.10 \pm 0.15	95.23 \pm 0.19	94.92 \pm 0.11	50.86 \pm 0.10	21.74 \pm 0.15	61.82 \pm 0.17	46.52 \pm 0.16	
DMGC	95.40 \pm 0.15	94.83 \pm 0.10	90.36 \pm 0.13	90.24 \pm 0.15	49.62 \pm 0.23	22.23 \pm 0.16	62.15 \pm 0.15	48.71 \pm 0.15	
DGF	95.50 \pm 0.14	96.33 \pm 0.16	97.88 \pm 0.11	97.74 \pm 0.14	47.35 \pm 0.20	18.36 \pm 0.24	64.50 \pm 0.11	48.83 \pm 0.15	
MIG-GT	95.04 \pm 0.12	94.50 \pm 0.15	92.60 \pm 0.17	92.87 \pm 0.12	52.58 \pm 0.18	25.49 \pm 0.21	65.45 \pm 0.15	48.93 \pm 0.19	
LGMRec	99.80 \pm 0.10	99.75 \pm 0.13	99.84 \pm 0.15	99.87 \pm 0.10	52.83 \pm 0.16	21.34 \pm 0.19	64.67 \pm 0.15	48.12 \pm 0.15	
UniGraph2	96.46 \pm 0.12	96.52 \pm 0.23	97.83 \pm 0.15	97.71 \pm 0.21	49.51 \pm 0.18	20.86 \pm 0.16	64.77 \pm 0.19	47.33 \pm 0.15	
CAMPA	99.69 \pm 0.15	99.50 \pm 0.17	99.89 \pm 0.12	99.79 \pm 0.15	53.16 \pm 0.21	23.24 \pm 0.25	66.41 \pm 0.13	49.92 \pm 0.20	

Table 3: Ablation study on representative tasks.

Tasks	Node Classification		Link Prediction		Modality Retrieval		G2Image	
Variants	Goodreads		Cloth		RedditS		Bili_music	
	Acc	F1	MRR	Hits@3	T2I-MRR	I2T-MRR	CLIP	DINOv2
w/o CAP	71.18 \pm 0.24	65.31 \pm 0.23	56.52 \pm 0.19	63.33 \pm 0.25	96.33 \pm 0.16	96.72 \pm 0.22	50.42 \pm 0.20	20.95 \pm 0.21
w/o TAA	72.66 \pm 0.27	65.76 \pm 0.33	57.11 \pm 0.25	63.91 \pm 0.19	97.52 \pm 0.17	97.14 \pm 0.21	51.23 \pm 0.19	21.98 \pm 0.23
w/o SA	73.31 \pm 0.23	66.30 \pm 0.20	58.61 \pm 0.22	64.91 \pm 0.16	98.16 \pm 0.20	98.35 \pm 0.21	52.46 \pm 0.24	22.63 \pm 0.28
w/o CA	72.98 \pm 0.27	66.63 \pm 0.22	58.32 \pm 0.20	64.33 \pm 0.16	97.96 \pm 0.18	98.02 \pm 0.20	51.69 \pm 0.21	22.01 \pm 0.19
CAMPA	76.93 \pm 0.20	67.29 \pm 0.22	60.33 \pm 0.30	68.17 \pm 0.24	99.89 \pm 0.12	99.79 \pm 0.15	53.16 \pm 0.21	23.24 \pm 0.25

4.3 Ablation Study

To answer **Q3**, we conduct a comprehensive ablation study. The core question is whether stage-wise alignment is necessary at both stages, and whether the detailed design of trajectory interaction and modality-specific hop fusion is justified. We consider the following variants, where SA and CA denote self-attention and cross-attention in TAA, respectively: (1) w/o CAP, where cross-modal aligned propagation is removed; (2) w/o TAA, where trajectory aligned aggregation is replaced by a simple trajectory fusion module; (3) w/o SA, where intra-modal trajectory encoding is removed; (4) w/o CA, where inter-modal trajectory interaction is removed; (5) full CAMPA.

The results in Table 3 show that removing either CAP or TAA degrades all metrics, confirming that modal conflict should be handled in both propagation and aggregation stages. Among the variants, w/o CAP causes the largest average drop, including 5.75 in accuracy on Goodreads and 4.84 in Hits@3 on Cloth. This suggests that injecting cross-modal semantic priors during diffusion is critical for preventing modality discrepancy from being amplified along multi-hop propagation. w/o TAA also clearly underperforms full CAMPA, indicating that aligned propagation trajectories still need trajectory-level interaction before fusion. In addition, removing self-attention or cross-attention in TAA consistently weakens the results: w/o SA mainly affects graph-centric metrics, while w/o CA produces larger average degradation and is more harmful to modality-centric tasks. These observations demonstrate that CAP and TAA are complementary, with CAP constructing aligned multi-hop trajectories and TAA coordinating intra-modal and inter-modal correspondence.

4.4 Running Efficiency

To answer **Q4**, efficiency is a key motivation for using a decoupled architecture. Fig. 3 compares the performance-time trajectories of CAMPA and representative baselines on four dataset-task pairs, where the horizontal axis records wall-clock training time and the vertical axis reports the corresponding task metric. Across all tasks, CAMPA rapidly enters the high-performance region and remains the best or highly competitive throughout training. In contrast, SIGN is lightweight but saturates at a lower level, while stronger multimodal baselines such as UniGraph2 and MIG-GT generally require longer training and often remain below CAMPA under comparable time budgets.

These results confirm that CAMPA preserves the lightweight optimization pattern of decoupled MAG models while substantially improving their representational quality. The advantage is especially

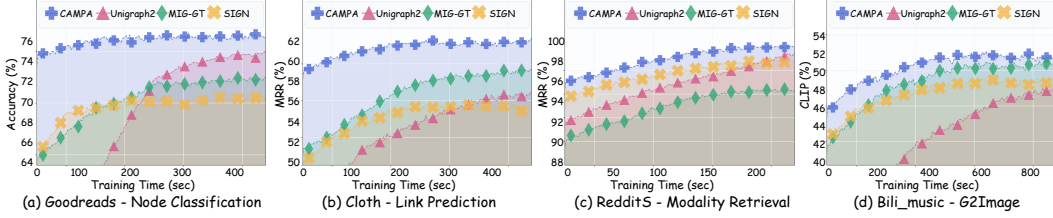


Figure 3: Efficiency analysis on four representative dataset-task pairs. Each subplot reports task performance against wall-clock training time. CAMPA consistently achieves a favorable performance-time trade-off across graph-centric and modality-centric tasks.

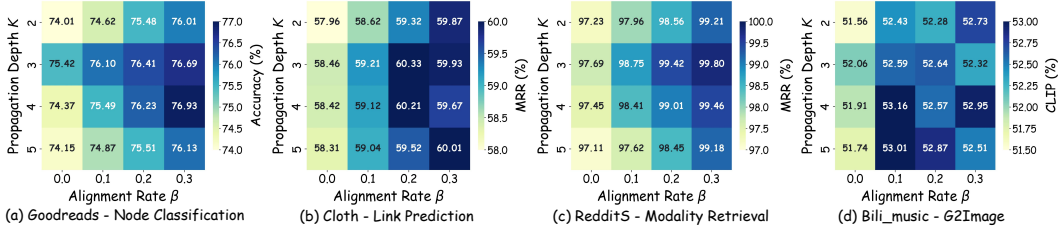


Figure 4: Hyperparameter sensitivity with respect to propagation depth K and alignment rate β . Each heatmap reports the task metric on one representative dataset-task pair. CAMPA achieves stable performance across a broad range of moderate alignment rates and propagation depths.

meaningful because CAMPA does not obtain higher accuracy by relying on a deeply coupled propagation process; instead, it injects alignment at the propagation and aggregation stages with limited additional cost. Therefore, CAMPA provides a practical efficiency-performance trade-off for scalable MAG learning, complementing the complexity analysis in Appendix C.

4.5 Hyperparameter Sensitivity

To answer **Q5**, we examine the sensitivity of CAMPA to two key hyperparameters: the propagation depth K and the alignment rate β that controls the strength of cross-modal propagation. Fig. 4 reports heatmaps on four representative dataset-task pairs, covering both graph-centric and modality-centric settings. Across all datasets, setting $\beta = 0$ usually leads to weaker performance, confirming that cross-modal propagation is important for effective decoupled MAG learning. Increasing β to a moderate positive range consistently improves the results, while the best region is generally broad rather than concentrated at a single configuration. The effect of K shows a similar pattern: shallow propagation may miss useful higher-order context, whereas overly deep propagation can introduce redundant or noisy signals. Overall, CAMPA performs stably around $K = 3$ or 4 with $\beta \in [0.1, 0.3]$, indicating that its gains do not rely on a narrow hyperparameter choice.

5 Conclusion

In this work, we propose CAMPA, a decoupled MAG framework that addresses modal conflict at both the propagation and aggregation stages. Motivated by our empirical observations that decoupled MAG learning is scalable yet prone to insufficient cross-modal coordination, CAMPA introduces CAP to inject cross-modal semantic priors into graph diffusion and TAA to align multi-hop trajectories before hop fusion. This design preserves the efficiency advantages of decoupled propagation while improving modality alignment and downstream representation quality. Theoretical analysis further supports the stability of aligned propagation and the discrepancy-controlled behavior of trajectory fusion. Extensive experiments across graph-centric and modality-centric tasks demonstrate that CAMPA consistently improves over coupled, decoupled, and recent multimodal graph baselines, while retaining favorable efficiency. These results highlight stage-wise alignment as an effective principle for scalable multimodal graph learning. Future work may extend CAMPA to richer modality combinations, stronger generative settings, and more adaptive large-scale MAG benchmarks.

References

- [1] Tian Bian, Xi Xiao, Tingyang Xu, Peilin Zhao, Wenbing Huang, Yu Rong, and Junzhou Huang. Rumor detection on social media with bi-directional graph convolutional networks. In *Proceedings of the Association for the Advancement of Artificial Intelligence, AAAI*, 2020.
- [2] Shaked Brody, Uri Alon, and Eran Yahav. How attentive are graph attention networks? *International Conference on Learning Representations, ICLR*, 2022.
- [3] Jie Cai, Xin Wang, Haoyang Li, Ziwei Zhang, and Wenwu Zhu. Multimodal graph neural architecture search under distribution shifts. In *Proceedings of the AAAI Conference on Artificial Intelligence, AAAI*, 2024.
- [4] Jinsong Chen, Kaiyuan Gao, Gaichao Li, and Kun He. Nagphormer: A tokenized graph transformer for node classification in large graphs. In *International Conference on Learning Representations, ICLR*, 2023.
- [5] Ming Chen, Zhewei Wei, Zengfeng Huang, Bolin Ding, and Yaliang Li. Simple and deep graph convolutional networks. In *International Conference on Machine Learning, ICML*, 2020.
- [6] Karan Desai, Gaurav Kaul, Zubin Trivadi Aysola, and Justin Johnson. Redcaps: Web-curated image-text data created by the people, for the people. In *Advances in Neural Information Processing Systems, NeurIPS Datasets and Benchmarks Track*, 2021.
- [7] Dongzhe Fan, Yi Fang, Jiajin Liu, Djellel Difallah, and Qiaoyu Tan. Mlaga: Multimodal large language and graph assistant. *arXiv preprint arXiv:2506.02568*, 2025.
- [8] Yi Fang, Bowen Jin, Jiacheng Shen, Sirui Ding, Qiaoyu Tan, and Jiawei Han. Graphgpt-o: Synergistic multimodal comprehension and generation on graphs. In *Proceedings of the Computer Vision and Pattern Recognition Conference, CVPR*, pages 19467–19476, 2025.
- [9] Fabrizio Frasca, Emanuele Rossi, Davide Eynard, Ben Chamberlain, Michael Bronstein, and Federico Monti. Sign: Scalable inception graph neural networks. *arXiv preprint arXiv:2004.11198*, 2020.
- [10] Noa Garcia and George Vogiatzis. How to read paintings: semantic art understanding with multimodal retrieval. In *Proceedings of the European Conference on Computer Vision Workshops, ECCV*, 2018.
- [11] Zhaochen Guo, Zhixiang Shen, Xuanting Xie, Liangjian Wen, and Zhao Kang. Disentangling homophily and heterophily in multimodal graph clustering. *CoRR*, abs/2507.15253, 2025.
- [12] Zhiqiang Guo, Jianjun Li, Guohui Li, Chaoyang Wang, Si Shi, and Bin Ruan. Lgmrec: Local and global graph learning for multimodal recommendation. In *AAAI*, pages 8454–8462. AAAI Press, 2024.
- [13] Yufei He, Yuan Sui, Xiaoxin He, Yue Liu, Yifei Sun, and Bryan Hooi. Unigraph2: Learning a unified embedding space to bind multimodal graphs. *arXiv preprint arXiv:2502.00806*, 2025.
- [14] Yupeng Hou, Jiacheng Li, Zhankui He, An Yan, Xiushi Chen, and Julian McAuley. Bridging language and items for retrieval and recommendation. *arXiv preprint arXiv:2403.03952*, 2024.
- [15] Jun Hu, Yufei He, Yuan Li, Bryan Hooi, and Bingsheng He. Ntsformer: A self-teaching graph transformer for multimodal isolated cold-start node classification. In *Proceedings of the AAAI Conference on Artificial Intelligence, AAAI*, 2025.
- [16] Jun Hu, Bryan Hooi, Bingsheng He, and Yinwei Wei. Modality-independent graph neural networks with global transformers for multimodal recommendation. In *AAAI*, pages 11790–11798. AAAI Press, 2025.
- [17] Jun Hu, Bryan Hooi, Shengsheng Qian, Quan Fang, and Changsheng Xu. Mgdcf: Distance learning via markov graph diffusion for neural collaborative filtering. *IEEE Transactions on Knowledge and Data Engineering*, 36(7):3281–3296, 2024.

- [18] Bowen Jin, Ziqi Pang, Bingjun Guo, Yu-Xiong Wang, Jiaxuan You, and Jiawei Han. Instructg2i: Synthesizing images from multimodal attributed graphs. *Advances in Neural Information Processing Systems*, 37:117614–117635, 2024.
- [19] Thomas N Kipf and Max Welling. Semi-supervised classification with graph convolutional networks. In *International Conference on Learning Representations, ICLR*, 2017.
- [20] Yunqing Li, Zixiang Tang, Jiaying Zhuang, Zhenyu Yang, Farhad Ameri, and Jianbang Zhang. C-mag: Cascade multimodal attributed graphs for supply chain link prediction. In *Proceedings of the KDD Workshop on AI for Supply Chain*, 2025.
- [21] Jiajin Liu, Dongzhe Fan, Jiacheng Shen, Chuanhao Ji, Daochen Zha, and Qiaoyu Tan. Graph-mlm: Harnessing multimodal large language models for multimodal graph learning. *arXiv preprint arXiv:2506.10282*, 2025.
- [22] Jianmo Ni, Jiacheng Li, and Julian McAuley. Justifying recommendations using distantly-labeled reviews and fine-grained aspects. In *Proceedings of the 2019 Conference on Empirical Methods in Natural Language Processing and the 9th International Joint Conference on Natural Language Processing (EMNLP-IJCNLP)*, pages 188–197. Association for Computational Linguistics, 2019.
- [23] Jianmo Ni, Jiacheng Li, and Julian McAuley. Justifying recommendations using distantly-labeled reviews and fine-grained aspects. In *Proceedings of the Conference on Empirical Methods in Natural Language Processing and the International Joint Conference on Natural Language Processing, EMNLP-IJCNLP*, 2019.
- [24] Xuying Ning, Dongqi Fu, Tianxin Wei, Wujiang Xu, and Jingrui He. Graph4mm: Weaving multimodal learning with structural information. In *Proceedings of the International Conference on Machine Learning, ICML*, 2025.
- [25] Maxime Oquab, Timothée Darcet, Theo Moutakanni, Huy V Vo, Marc Szafraniec, Vasil Khalidov, Pierre Fernandez, Daniel Haziza, Francisco Massa, Alaa El-Nouby, et al. Dinov2: Learning robust visual features without supervision. In *Transactions on Machine Learning Research, TMLR*, 2024.
- [26] Alec Radford, Jong Wook Kim, Chris Hallacy, Aditya Ramesh, Gabriel Goh, Sandhini Agarwal, Girish Sastry, Amanda Askell, Pamela Mishkin, Jack Clark, et al. Learning transferable visual models from natural language supervision. In *International Conference on Machine Learning, ICML*, 2021.
- [27] Zhulin Tao, Yinwei Wei, Xiang Wang, Xiangnan He, Xianglin Huang, and Tat-Seng Chua. MGAT: multimodal graph attention network for recommendation. *Inf. Process. Manag.*, 57(5):102277, 2020.
- [28] Petar Veličković, Guillem Cucurull, Arantxa Casanova, Adriana Romero, Pietro Lio, and Yoshua Bengio. Graph attention networks. In *International Conference on Learning Representations, ICLR*, 2018.
- [29] Chenxi Wan, Xunkai Li, Yilong Zuo, Haokun Deng, Sihan Li, Bowen Fan, Hongchao Qin, Ronghua Li, and Guoren Wang. Openmag: A comprehensive benchmark for multimodal-attributed graph. *arXiv preprint arXiv:2602.05576*, 2026.
- [30] Mengting Wan and Julian McAuley. Item recommendation on monotonic behavior chains. In *Proceedings of the ACM Conference on Recommender Systems, RecSys*, 2018.
- [31] Mengting Wan, Rishabh Misra, Ndapandula Nakashole, and Julian McAuley. Fine-grained spoiler detection from large-scale review corpora. In *Proceedings of the Annual Meeting of the Association for Computational Linguistics, ACL*, 2019.
- [32] Peng Wang, Shuai Bai, Sinan Tan, Shijie Wang, Zhihao Fan, Jinze Bai, Keqin Chen, Xuejing Liu, Jialin Wang, Wenbin Ge, Yang Fan, Kai Dang, Mengfei Du, Xuancheng Ren, Rui Men, Dayiheng Liu, Chang Zhou, Jingren Zhou, and Junyang Lin. Qwen2-vl: Enhancing vision-language model’s perception of the world at any resolution, 2024.

- [33] Xin Wang, Zeyang Zhang, Linxin Xiao, Haibo Chen, Chendi Ge, and Wenwu Zhu. Towards multi-modal graph large language model. *arXiv preprint arXiv:2506.09738*, 2025.
- [34] Yinwei Wei, Xiang Wang, Liqiang Nie, Xiangnan He, Richang Hong, and Tat-Seng Chua. MMGCN: multi-modal graph convolution network for personalized recommendation of micro-video. In *ACM Multimedia*, pages 1437–1445. ACM, 2019.
- [35] Felix Wu, Amauri Souza, Tianyi Zhang, Christopher Fifty, Tao Yu, and Kilian Weinberger. Simplifying graph convolutional networks. In *International Conference on Machine Learning, ICML*, 2019.
- [36] Zonghan Wu, Shirui Pan, Fengwen Chen, Guodong Long, Chengqi Zhang, and S Yu Philip. A comprehensive survey on graph neural networks. *IEEE Transactions on Neural Networks and Learning Systems*, 32(1):4–24, 2020.
- [37] Hao Yan, Chaozhuo Li, Jun Yin, Zhigang Yu, Weihao Han, Mingzheng Li, Zhengxin Zeng, Hao Sun, and Senzhang Wang. When graph meets multimodal: benchmarking and meditating on multimodal attributed graph learning. In *Proceedings of the ACM SIGKDD Conference on Knowledge Discovery and Data Mining, KDD*, 2025.
- [38] Minji Yoon, Jing Yu Koh, Bryan Hooi, and Ruslan Salakhutdinov. Multimodal graph learning for generative tasks. *arXiv preprint arXiv:2310.07478*, 2023.
- [39] Wentao Zhang, Mingyu Yang, Zeang Sheng, Yang Li, Wen Ouyang, Yangyu Tao, Zhi Yang, and Bin Cui. Node dependent local smoothing for scalable graph learning. *Advances in Neural Information Processing Systems, NeurIPS*, 2021.
- [40] Wentao Zhang, Ziqi Yin, Zeang Sheng, Yang Li, Wen Ouyang, Xiaosen Li, Yangyu Tao, Zhi Yang, and Bin Cui. Graph attention multi-layer perceptron. *Proceedings of the ACM SIGKDD Conference on Knowledge Discovery and Data Mining, KDD*, 2022.
- [41] Haoran Zheng, Renchi Yang, Hongtao Wang, and Jianliang Xu. Cross-contrastive clustering for multimodal attributed graphs with dual graph filtering, 2025.
- [42] Yu Zhou, Haixia Zheng, Xin Huang, Shufeng Hao, Dengao Li, and Jumin Zhao. Graph neural networks: Taxonomy, advances, and trends. *ACM Transactions on Intelligent Systems and TechnoLoGy*, 13(1):1–54, 2022.
- [43] Jing Zhu, Yuhang Zhou, Shengyi Qian, Zhongmou He, Tong Zhao, Neil Shah, and Danai Koutra. Mosaic of modalities: A comprehensive benchmark for multimodal graph learning. In *Proceedings of the Computer Vision and Pattern Recognition Conference, CVPR*, 2025.

A Supplementary Empirical Analysis

This appendix supplements the empirical studies in Sec. 1 and provides additional details on the efficiency comparison between coupled and decoupled architectures as well as the modal conflict phenomenon in decoupled multimodal graph learning.

A.1 Setup of Empirical Studies

Empirical Study (a): Coupled vs. Decoupled Architectures. We compare representative coupled baselines, namely MGAT and MMGCN, against representative decoupled baselines, including MSGC, SIGN, and MGDN, on the Toys dataset under the node classification setting. MSGC is our in-house multimodal adaptation of SGC [35]. Specifically, we extend the decoupled propagate-then-classify paradigm to the multimodal setting by performing modality-wise graph propagation on text and image features, followed by a shared prediction module for downstream classification. For fairness, MSGC uses the same input features, training budget, and evaluation protocol as the other baselines. The Toys dataset is extracted from the "Toys & Games" category of Amazon2018 [22]. All methods use the same input modalities, train/validation/test split, and evaluation protocol, while their training time is recorded under the same hardware environment. We report the accuracy-time trajectories throughout training to jointly examine predictive performance and computational efficiency.

Empirical Study (b): Stage-wise Alignment Analysis. To investigate whether modal conflict is an intrinsic issue in decoupled pipelines, we augment representative decoupled baselines with lightweight alignment modules at different stages, including propagation-stage alignment (AlignP), aggregation-stage alignment (AlignA), and their combination. Consistent improvements brought by these lightweight alignment modules would indicate that the corresponding stage indeed suffers from insufficient multimodal interaction.

Propagation-stage alignment (AlignP). Let $\{\mathbf{H}_t^{(k)}\}_{k=0}^K$ and $\{\mathbf{H}_i^{(k)}\}_{k=0}^K$ denote the text and image trajectories produced by a generic decoupled baseline. AlignP injects lightweight same-hop cross-modal correction during propagation:

$$\widehat{\mathbf{H}}_t^{(k)} = (1 - \lambda_p)\mathbf{H}_t^{(k)} + \lambda_p\mathbf{P}_{i \rightarrow t}\mathbf{H}_i^{(k)}, \quad \widehat{\mathbf{H}}_i^{(k)} = (1 - \lambda_p)\mathbf{H}_i^{(k)} + \lambda_p\mathbf{P}_{t \rightarrow i}\mathbf{H}_t^{(k)}, \quad (16)$$

where $\mathbf{P}_{i \rightarrow t}$ and $\mathbf{P}_{t \rightarrow i}$ are lightweight learnable projections used only to match the feature spaces, and λ_p controls the strength of propagation-stage alignment. This design preserves the decoupled structure of the baseline while introducing a minimal form of cross-modal interaction during multi-hop diffusion.

Aggregation-stage alignment (AlignA). AlignA leaves the propagation stage unchanged and introduces coordination only when the baseline aggregates the multi-hop trajectories. Let $\text{Agg}(\cdot)$ denote the original hop aggregation operator of the decoupled baseline. We first obtain modality-specific aggregated embeddings:

$$\mathbf{z}_t = \text{Agg}\left(\{\mathbf{H}_t^{(k)}\}_{k=0}^K\right), \quad \mathbf{z}_i = \text{Agg}\left(\{\mathbf{H}_i^{(k)}\}_{k=0}^K\right), \quad (17)$$

and then apply a lightweight cross-modal refinement:

$$\widehat{\mathbf{z}}_t = (1 - \lambda_a)\mathbf{z}_t + \lambda_a\mathbf{Q}_{i \rightarrow t}\mathbf{z}_i, \quad \widehat{\mathbf{z}}_i = (1 - \lambda_a)\mathbf{z}_i + \lambda_a\mathbf{Q}_{t \rightarrow i}\mathbf{z}_t, \quad (18)$$

where $\mathbf{Q}_{i \rightarrow t}$ and $\mathbf{Q}_{t \rightarrow i}$ are lightweight learnable projections and λ_a controls the strength of aggregation-stage alignment. The final fused representation is then formed as $\widehat{\mathbf{z}} = \widehat{\mathbf{z}}_t \parallel \widehat{\mathbf{z}}_i$. Compared with AlignP, this module does not alter the diffusion process and only improves the coordination of the final multimodal summaries.

Combined alignment. For the +AlignP+AlignA setting, we first apply AlignP to obtain aligned trajectories $\{\widehat{\mathbf{H}}_t^{(k)}\}$ and $\{\widehat{\mathbf{H}}_i^{(k)}\}$, and then apply AlignA on top of the corresponding aggregated embeddings. This setting examines whether propagation-stage and aggregation-stage coordination are complementary.

Visualization and measurement. Beyond the quantitative gains shown in Fig. 1(b), we further provide heatmap-based correlation analysis and t-SNE visualizations in Appendix A.2 to illustrate how alignment affects cross-modal consistency and latent-space geometry.

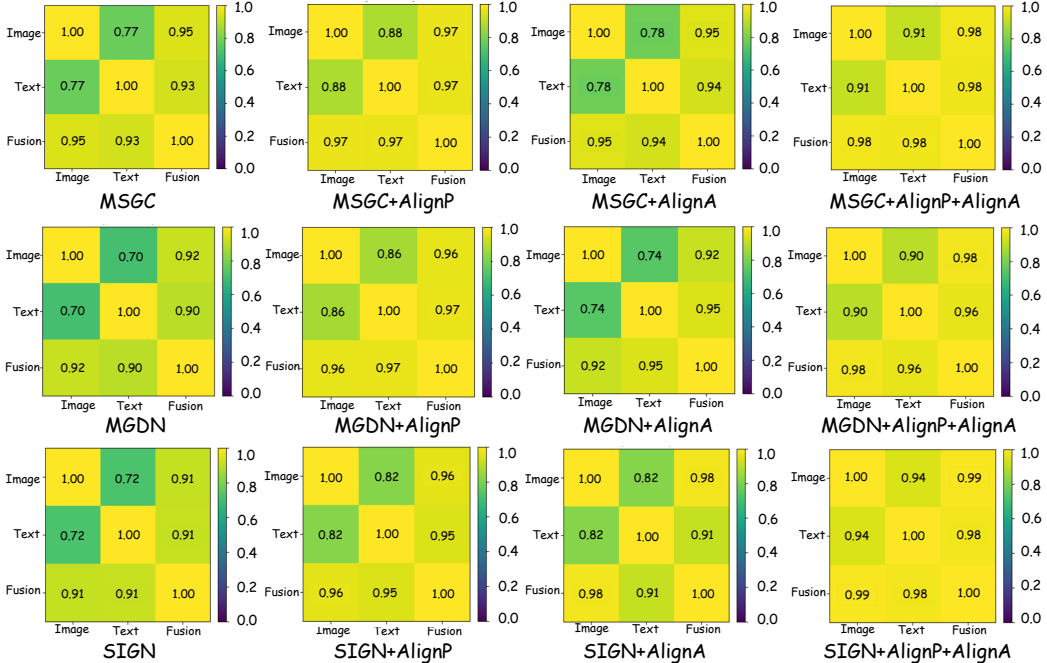


Figure 5: Heatmap visualization of cross-modal feature correlations. From top to bottom, we show the results of MSGC, MGDN, and SIGN. Within each row, (a) denotes the original decoupled baseline, (b) augments it with propagation-stage alignment, (c) augments it with aggregation-stage alignment, and (d) applies both alignment modules together.

A.2 Visual Analysis of Modal Conflict

To further support the empirical study (b) in Sec. 1, we provide additional evidence on the modal conflict phenomenon. These visualizations show how the lack of cross-modal coordination leads to representation inconsistency, and how stage-wise alignment progressively alleviates this issue.

Visualization protocol. We analyze representative decoupled baselines under four settings, including the original model, propagation-stage alignment (+AlignP), aggregation-stage alignment (+AlignA), and their combination (+AlignP+AlignA). For each baseline, we report two complementary forms of visualization. The first is a heatmap of pairwise feature correlations among image, text, and fused representations, which reflects the degree of cross-modal consistency in the learned space. The second is a t-SNE visualization of image and text embeddings, which reveals whether the two modalities remain spatially separated or become progressively aligned after introducing stage-wise coordination.

Heatmap analysis. Fig. 5 presents the heatmap-based comparison. The top, middle, and bottom rows correspond to MSGC, MGDN, and SIGN, respectively. For MSGC, the original model exhibits relatively weak Image-Text correlation, whereas AlignP substantially improves the correlation structure and AlignP+AlignA yields the strongest overall consistency. The same trend can also be observed on MGDN and SIGN, where the original model starts from a modality discrepancy, and both alignment modules improve the correlation between modality-specific and fused representations. Overall, the combined variant consistently produces the strongest cross-modal consistency, indicating that modal conflict exists in decoupled pipelines and can be reduced by stage-wise alignment.

T-SNE analysis. Fig. 6 further provides a geometric view of the same phenomenon. For MSGC, MGDN, and SIGN, the original models produce clearly separated image and text clusters, suggesting that the two modalities evolve in different semantic spaces when propagated and aggregated independently. After introducing AlignP, the two modality distributions become substantially more mixed, showing that propagation-stage coordination can directly reduce spatial asynchrony. Adding AlignA also improves the overlap, while the full variant with AlignP+AlignA yields the most coherent multimodal geometry. These observations further verify that the empirical gains in Fig. 1(b) originate from a genuine reduction of modal conflict rather than incidental optimization effects.

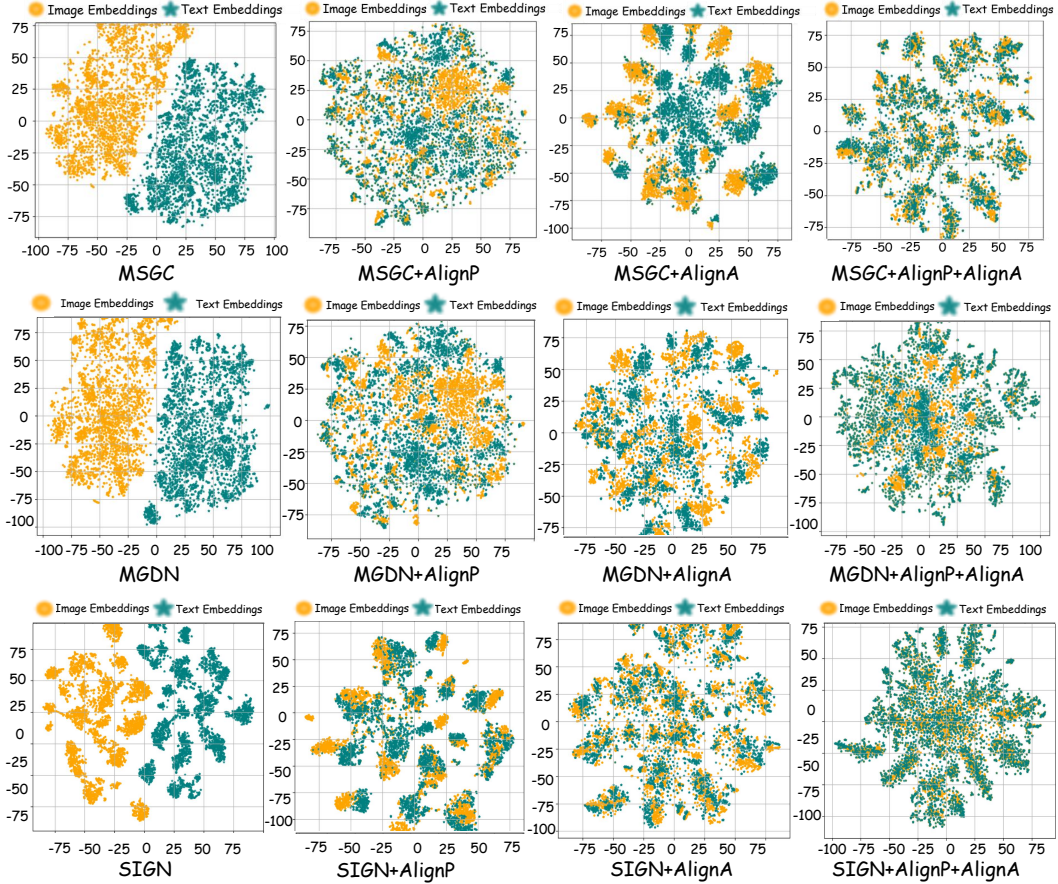


Figure 6: T-SNE visualization of image and text embeddings. From top to bottom, we show the results of MSGC, MGDN, and SIGN. The original decoupled models exhibit obvious modality separation, whereas stage-wise alignment progressively increases the overlap between image and text embeddings.

Discussion. Taken together, the heatmap and t-SNE results offer a more intuitive explanation of the empirical study in Sec. 1. They show that modal conflict in decoupled MGNNs is reflected not only in final performance degradation, but also in weak representation-level correlation and clear geometric separation between modalities. More importantly, they also show that the two alignment modules play complementary roles: *AlignP* mainly improves cross-modal consistency during propagation, while *AlignA* further refines the coordination of multimodal trajectories during aggregation. This provides direct motivation for the two-stage design of CAMPA.

B Proofs of Theoretical Analysis

This appendix provides detailed proofs for the theoretical results in Sec. 3.3. We first prove the convergence and boundedness of CAP, and then establish the bounded and discrepancy-controlled property of TAA.

B.1 Proof of Theorem 3.1

We restate the CAP recursion:

$$\mathbf{X}^{(k+1)} = \mathbf{P}\mathbf{X}^{(k)} + \mathbf{R}\mathbf{X}^{(0)}, \quad (19)$$

where \mathbf{P} and \mathbf{R} are defined in Eq. (10). For any block vector $\mathbf{X} = [\mathbf{X}_t; \mathbf{X}_i]$, recall the norm

$$\|\mathbf{X}\|_{2,\infty} = \max(\|\mathbf{X}_t\|_F, \|\mathbf{X}_i\|_F).$$

Proof. Since each $\tilde{\mathbf{A}}_{uv}$ is symmetrically normalized, we have $\|\tilde{\mathbf{A}}_{uv}\|_2 \leq 1$. Therefore, for any $\mathbf{X} = [\mathbf{X}_t; \mathbf{X}_i]$,

$$\mathbf{P}\mathbf{X} = \begin{bmatrix} \alpha_t \tilde{\mathbf{A}}_{tt} \mathbf{X}_t + \beta_t \tilde{\mathbf{A}}_{ti} \mathbf{X}_i \\ \beta_i \tilde{\mathbf{A}}_{it} \mathbf{X}_t + \alpha_i \tilde{\mathbf{A}}_{ii} \mathbf{X}_i \end{bmatrix}. \quad (20)$$

Applying the submultiplicativity of the Frobenius norm yields

$$\begin{aligned} \|\alpha_t \tilde{\mathbf{A}}_{tt} \mathbf{X}_t + \beta_t \tilde{\mathbf{A}}_{ti} \mathbf{X}_i\|_F &\leq \alpha_t \|\tilde{\mathbf{A}}_{tt} \mathbf{X}_t\|_F + \beta_t \|\tilde{\mathbf{A}}_{ti} \mathbf{X}_i\|_F \\ &\leq \alpha_t \|\mathbf{X}_t\|_F + \beta_t \|\mathbf{X}_i\|_F \\ &\leq (\alpha_t + \beta_t) \|\mathbf{X}\|_{2,\infty}, \end{aligned} \quad (21)$$

and similarly,

$$\|\beta_i \tilde{\mathbf{A}}_{it} \mathbf{X}_t + \alpha_i \tilde{\mathbf{A}}_{ii} \mathbf{X}_i\|_F \leq (\alpha_i + \beta_i) \|\mathbf{X}\|_{2,\infty}. \quad (22)$$

Combining Eqs. (21) and (22), we obtain

$$\|\mathbf{P}\mathbf{X}\|_{2,\infty} \leq \rho \|\mathbf{X}\|_{2,\infty}, \quad \rho = \max(\alpha_t + \beta_t, \alpha_i + \beta_i). \quad (23)$$

Hence, if $\rho < 1$, \mathbf{P} is a contraction under $\|\cdot\|_{2,\infty}$.

The fixed point \mathbf{X}^* of Eq. (19) satisfies

$$\mathbf{X}^* = \mathbf{P}\mathbf{X}^* + \mathbf{R}\mathbf{X}^{(0)}, \quad (24)$$

which is equivalent to

$$(\mathbf{I} - \mathbf{P})\mathbf{X}^* = \mathbf{R}\mathbf{X}^{(0)}. \quad (25)$$

Since $\rho < 1$, the matrix $\mathbf{I} - \mathbf{P}$ is invertible and thus the fixed point is unique:

$$\mathbf{X}^* = (\mathbf{I} - \mathbf{P})^{-1} \mathbf{R}\mathbf{X}^{(0)}. \quad (26)$$

Subtracting Eq. (24) from Eq. (19) gives

$$\mathbf{X}^{(k+1)} - \mathbf{X}^* = \mathbf{P}(\mathbf{X}^{(k)} - \mathbf{X}^*). \quad (27)$$

Taking the block norm on both sides and using Eq. (23), we obtain

$$\|\mathbf{X}^{(k+1)} - \mathbf{X}^*\|_{2,\infty} \leq \rho \|\mathbf{X}^{(k)} - \mathbf{X}^*\|_{2,\infty}, \quad (28)$$

which proves the linear convergence claim in Theorem 3.1.

For completeness, we further bound the magnitude of the fixed point. From Eq. (24),

$$\|\mathbf{X}^*\|_{2,\infty} \leq \|\mathbf{P}\mathbf{X}^*\|_{2,\infty} + \|\mathbf{R}\mathbf{X}^{(0)}\|_{2,\infty} \leq \rho \|\mathbf{X}^*\|_{2,\infty} + \max(\gamma_t, \gamma_i) \|\mathbf{X}^{(0)}\|_{2,\infty}. \quad (29)$$

Rearranging yields

$$\|\mathbf{X}^*\|_{2,\infty} \leq \frac{\max(\gamma_t, \gamma_i)}{1 - \rho} \|\mathbf{X}^{(0)}\|_{2,\infty}. \quad (30)$$

This completes the proof. \square

B.2 Proof of Proposition 3.2

For one node, recall that

$$\mathbf{z}_u = \sum_{k=0}^K a_u^{(k)} \mathbf{g}_u^{(k)}, \quad u \in \{t, i\}, \quad (31)$$

where $a_u^{(k)} \geq 0$ and $\sum_{k=0}^K a_u^{(k)} = 1$.

Proof. Because $\{a_u^{(k)}\}_{k=0}^K$ are nonnegative and sum to one, \mathbf{z}_u is a convex combination of $\{\mathbf{g}_u^{(0)}, \dots, \mathbf{g}_u^{(K)}\}$. Therefore, $\mathbf{z}_u \in \text{conv}\{\mathbf{g}_u^{(0)}, \dots, \mathbf{g}_u^{(K)}\}$. Applying the triangle inequality gives

$$\|\mathbf{z}_u\|_2 = \left\| \sum_{k=0}^K a_u^{(k)} \mathbf{g}_u^{(k)} \right\|_2 \leq \sum_{k=0}^K a_u^{(k)} \|\mathbf{g}_u^{(k)}\|_2 \leq \max_{0 \leq k \leq K} \|\mathbf{g}_u^{(k)}\|_2, \quad (32)$$

Algorithm 1 Training Pipeline of CAMPA

Require: Graph adjacency \mathbf{A} , raw textual contents \mathcal{C}_t , raw visual contents \mathcal{C}_i , propagation depth K , balance coefficients α, β, γ , task supervision

Ensure: Trained TAA parameters and prediction head

- 1: Encode \mathcal{C}_t and \mathcal{C}_i with a frozen pre-trained vision-language encoder to obtain initial modality features $\mathbf{H}_t^{(0)}$ and $\mathbf{H}_i^{(0)}$.
- 2: **Offline aligned propagation**
- 3: Compute edge-wise semantic priors $\mathbf{S}_{tt}, \mathbf{S}_{ii}, \mathbf{S}_{ti}, \mathbf{S}_{it}$ and construct $\tilde{\mathbf{A}}_{tt}, \tilde{\mathbf{A}}_{ii}, \tilde{\mathbf{A}}_{ti}, \tilde{\mathbf{A}}_{it}$ by Eq. (1).
- 4: Initialize the trajectories with $\mathbf{H}_t^{(0)}$ and $\mathbf{H}_i^{(0)}$.
- 5: **for** $k = 0, \dots, K - 1$ **do**
- 6: Update $\mathbf{H}_t^{(k+1)}$ and $\mathbf{H}_i^{(k+1)}$ by Eq. (2).
- 7: **end for**
- 8: Stack the propagated slices to obtain $\mathbf{H}_t = [\mathbf{H}_t^{(0)}, \dots, \mathbf{H}_t^{(K)}]$ and $\mathbf{H}_i = [\mathbf{H}_i^{(0)}, \dots, \mathbf{H}_i^{(K)}]$.
- 9: **Online trajectory-aligned training**
- 10: **for** each training epoch **do**
- 11: Perform intra-modal trajectory encoding on \mathbf{H}_t and \mathbf{H}_i to obtain \mathbf{F}_t and \mathbf{F}_i by Eq. (4).
- 12: Apply inter-modal trajectory interaction to obtain \mathbf{G}_t and \mathbf{G}_i by Eq. (6).
- 13: Compute hop-wise consistency \mathbf{C} and modality-specific hop weights $\mathbf{A}_t, \mathbf{A}_i$ by Eqs. (7) and (8).
- 14: Aggregate \mathbf{Z}_t and \mathbf{Z}_i and form $\mathbf{Z} = \mathbf{Z}_t \parallel \mathbf{Z}_i$ by Eq. (9).
- 15: Optimize the TAA parameters and task head with the downstream loss.
- 16: **end for**
- 17: **Return** the trained CAMPA model.

which establishes the boundedness of \mathbf{z}_u as a convex combination of hop-wise representations.

Next, consider the difference between the two fused representations:

$$\begin{aligned} \mathbf{z}_t - \mathbf{z}_i &= \sum_{k=0}^K a_t^{(k)} \mathbf{g}_t^{(k)} - \sum_{k=0}^K a_i^{(k)} \mathbf{g}_i^{(k)} \\ &= \sum_{k=0}^K a_t^{(k)} (\mathbf{g}_t^{(k)} - \mathbf{g}_i^{(k)}) + \sum_{k=0}^K (a_t^{(k)} - a_i^{(k)}) \mathbf{g}_i^{(k)}. \end{aligned} \quad (33)$$

Taking the Euclidean norm and applying the triangle inequality yields

$$\begin{aligned} \|\mathbf{z}_t - \mathbf{z}_i\|_2 &\leq \left\| \sum_{k=0}^K a_t^{(k)} (\mathbf{g}_t^{(k)} - \mathbf{g}_i^{(k)}) \right\|_2 + \left\| \sum_{k=0}^K (a_t^{(k)} - a_i^{(k)}) \mathbf{g}_i^{(k)} \right\|_2 \\ &\leq \sum_{k=0}^K a_t^{(k)} \|\mathbf{g}_t^{(k)} - \mathbf{g}_i^{(k)}\|_2 + \sum_{k=0}^K |a_t^{(k)} - a_i^{(k)}| \|\mathbf{g}_i^{(k)}\|_2, \end{aligned} \quad (34)$$

which is exactly Eq. (15). The symmetric statement after swapping t and i follows from the same derivation. \square

C Algorithm and Complexity Analysis

This appendix summarizes the training pipeline of CAMPA and analyzes its computational complexity. Our goal is to make explicit which operations are precomputed in the aligned propagation stage and which operations remain in the online optimization stage.

C.1 Pseudo-code of CAMPA

Algorithm 1 highlights the decoupled nature of CAMPA. The graph-dependent aligned diffusion in CAP is executed once before training, whereas the online optimization stage only operates on the precomputed hop trajectories. This separation is the key reason why CAMPA retains the efficiency advantage of decoupled multimodal graph learning.

C.2 Complexity Analysis

Let N be the number of nodes, $|E|$ the number of observed edges, d the hidden dimension, K the propagation depth, and B the batch size used in the online training stage. For simplicity, we omit constant factors introduced by the two modalities and the four aligned propagation operators.

CAP precomputation. To construct the aligned operators in Eq. (1), CAMPA only needs semantic similarities on observed edges because the prior is multiplied by the sparse adjacency matrix \mathbf{A} . Computing the edge-wise semantic priors therefore costs $\mathcal{O}(|E|d)$, while symmetric normalization of the resulting sparse operators costs $\mathcal{O}(|E|)$. The subsequent K -hop aligned diffusion in Eq. (2) requires K sparse matrix-feature multiplications, leading to a total CAP precomputation cost of $\mathcal{O}(K|E|d)$. Storing the propagated trajectories for both modalities requires $\mathcal{O}(N(K+1)d)$ memory.

Online TAA training. Once the trajectories are precomputed, the online training stage no longer depends on the graph edges. For a batch of B nodes, the linear projections and MLP blocks in TAA cost $\mathcal{O}(B(K+1)d^2)$, while self-attention and cross-attention along the hop dimension cost $\mathcal{O}(B(K+1)^2d)$. The consistency scoring, gating, and weighted hop aggregation introduce an additional $\mathcal{O}(B(K+1)d)$ cost. Therefore, the per-epoch online complexity of CAMPA can be summarized as $\mathcal{O}(B(K+1)d^2 + B(K+1)^2d)$. Since K is typically small and fixed, the online training cost is independent of $|E|$ and scales only with the trajectory length and hidden dimension.

Overall efficiency advantage. Overall, the total cost of CAMPA consists of a one-time graph-dependent precomputation term and an edge-independent online optimization term. This is fundamentally different from coupled message-passing MGNNs, whose per-epoch training cost usually scales with repeated neighborhood aggregation over edges. By moving aligned diffusion to the precomputation stage, CAMPA preserves the efficiency benefits of decoupled training while still introducing explicit cross-modal coordination in both propagation and aggregation.

D Dataset Description

We evaluate CAMPA on eight multimodal graph datasets spanning recommendation, social, media, music, art, and book domains. Table 4 summarizes their modality composition, graph scale, label cardinality, representative task scope, and application domain used in our experiments.

Table 4: Statistics of the eight MAG datasets used in our experiments.

Dataset	Modalities	#Nodes	#Edges	#Classes	Task Scope	Domain
Ele-fashion	Text + Image	97,766	199,602	12	Graph + Modality	Recommendation
Bili_music	Text + Image	6,038	21,592	-	Graph + Modality	Video Recommendation
RedditS	Text + Image	15,894	566,160	20	Graph + Modality	Social Network
Movies	Text + Image	16,672	218,390	20	Graph + Modality	Movie Network
Goodreads	Text + Image	685,294	7,235,048	11	Graph	Book Network
Grocery	Text + Image	17,074	171,340	20	Graph + Modality	Recommendation
Cloth	Text + Image	125,839	951,271	-	Graph + Modality	Recommendation
SemArt	Text + Image	21,382	1,216,432	-	Graph + Modality	Art Network

Below we briefly describe each dataset used in our benchmark.

Ele-fashion [23, 14] is a heterogeneous product graph that combines Amazon electronics and fashion items. Nodes represent products and edges capture cross-category co-purchasing relations, revealing latent consumer preferences across distinct domains. Each node is associated with textual descriptions and product images, and the dataset supports both graph-centric and modality-centric evaluation.

Bili_music [29] is a music-content multimodal graph constructed from video or music-related entities. Its graph structure reflects content association and user-consumption correlation, while node attributes combine textual metadata with visual content. We mainly use this dataset to evaluate graph-aware multimodal understanding and retrieval behavior in content-oriented scenarios.

RedditS [6] is a social multimodal graph in which nodes correspond to Reddit posts and edges encode interaction or reply relations. The textual modality is derived from post titles and body content, while the visual modality comes from attached images. This dataset is particularly suitable for evaluating socially grounded node classification, clustering, and link prediction.

Movies [23] is a recommendation-style multimodal graph built on movie or media entities. Nodes contain textual descriptions and poster-like visual signals, while edges reflect semantic or behavioral relations among items. It provides a representative benchmark for studying multimodal graph learning in media recommendation settings.

Goodreads [30, 31] is a large-scale book graph where nodes represent books and edges encode user-behavior or shelving relations. Its textual modality captures summaries and editorial descriptions, whereas the visual modality is derived from book covers. The scale of this dataset makes it particularly useful for evaluating the scalability of efficient decoupled MAG methods.

Grocery [23] is a product graph from the recommendation domain, where edges describe complementary or co-purchasing patterns. Textual features reflect product titles and descriptions, while visual features come from product appearance or packaging images. This dataset is commonly used to evaluate cross-modal recommendation and alignment quality.

Cloth [23, 14] is a fashion-oriented recommendation graph that emphasizes visually sensitive item relations. Nodes contain both textual descriptions and clothing images, and edges reflect compatibility or co-consumption signals. The dataset is well suited for testing whether multimodal graph models can jointly capture semantic and visual compatibility.

SemArt [10] is an art-understanding benchmark where nodes correspond to artworks and edges encode semantic or metadata-based relations. Each node combines textual commentary with artwork images, providing a challenging testbed for graph-conditioned multimodal generation and alignment. We include it as a representative modality-centric benchmark, especially for graph-to-image related evaluation.

E Baseline Details

GAT [28] is a classical attention-based GNN that performs masked neighborhood aggregation with learnable edge attention coefficients. It can be viewed as a representative extension of early message-passing GNNs from convolution-style neighborhood smoothing to adaptive attention-based propagation [19, 2]. Although it is not designed for MAG learning, we include it as a general graph reference to calibrate the benefit of injecting multimodal information into graph representation learning. In our implementation, GAT receives the same graph structure and encoder-derived node features as the multimodal methods, so that the comparison isolates the gain from multimodal modeling rather than differences in raw inputs.

MMGCN [34] is one of the early representative multimodal graph models for recommendation. Its core design is to construct modality-specific graph encoders and then combine their outputs under shared graph supervision, thereby capturing complementary preference signals from different modalities. We include MMGCN because it represents a typical coupled MAG pipeline, in which message passing and multimodal fusion are tightly interleaved throughout training. This makes it a useful reference for assessing whether CAMPA can preserve the strengths of multimodal graph modeling while avoiding the efficiency limitations of coupled propagation.

MGAT [27] extends graph attention to multimodal recommendation by introducing gated attention mechanisms over graph neighbors and multimodal channels. Compared with MMGCN, MGAT places more emphasis on adaptive modality weighting during propagation and thus serves as another representative coupled MAG baseline with stronger interaction modeling capacity. We compare against MGAT to test whether CAMPA can still maintain an advantage when the baseline already performs nontrivial attention-based fusion inside the graph learning process.

DMGC [11] is a recent multimodal graph clustering method that explicitly disentangles homophily-oriented and heterophily-oriented graph patterns. It combines dual-branch structural modeling with multimodal fusion, aiming to improve clustering quality under complex graph semantics. We include DMGC because it is a strong modern baseline for graph-centric unsupervised MAG tasks and represents a design philosophy different from recommendation-oriented models. Its inclusion helps verify that CAMPA is not only competitive on recommendation benchmarks, but also remains effective on general representation learning scenarios.

DGF [41] adopts dual graph filtering together with cross-modal contrastive objectives to enhance robustness against noisy graph structure and modality corruption. Instead of relying on a single

propagation stream, DGF uses complementary filtered views to preserve informative low-frequency and high-frequency components. We include it as a recent strong baseline because it explicitly addresses noisy multimodal graph signals, which overlaps with part of the motivation behind our alignment-based design. This comparison is therefore important for showing that the improvements of CAMPA are not simply due to stronger denoising, but come from better stage-wise coordination across modalities.

MIG-GT [16] combines modality-independent graph encoders with a global transformer, thereby coupling local graph aggregation and long-range multimodal interaction in a unified framework. Its main appeal lies in balancing graph inductive bias with global dependency modeling, which makes it a strong reference for modern MAG architectures beyond purely local message passing. We compare against MIG-GT because it reflects a powerful coupled paradigm where multimodal coordination is handled through deep joint modeling rather than decoupled propagation.

LGMRec [12] is a representative lightweight multimodal recommendation model that integrates graph topology with modality-aware preference learning. It is particularly competitive in recommendation settings because it can effectively exploit user-item structural signals together with textual and visual content while maintaining relatively modest model complexity. We include LGMRec as a practical and task-oriented baseline, since it reflects the performance level of modern multimodal recommendation systems rather than purely generic MAG encoders.

UniGraph2 [13] learns a unified graph-aware embedding space that binds multiple modalities into a shared representation. Compared with earlier recommendation-focused methods, UniGraph2 emphasizes more general multimodal graph representation learning and stronger cross-modal semantic coupling. We treat it as a recent strong baseline because its unified embedding design is conceptually close to the broader goal of reducing modality discrepancy, making it a particularly meaningful comparator for CAMPA.

SIGN [9] is a classical decoupled GNN that precomputes multi-hop propagated features and performs downstream learning using lightweight predictors. Its key advantage is that graph diffusion is separated from trainable transformation, substantially reducing training cost on large graphs. Although SIGN itself is unimodal, it provides the canonical propagate-then-predict template for efficient decoupled graph learning. We therefore include it to evaluate whether the efficiency benefits of decoupling can be carried over to MAG scenarios without sacrificing multimodal modeling quality.

MSGC [35] denotes our multimodal adaptation of the SGC-style decoupled pipeline. Concretely, each modality is propagated independently over the graph to obtain multi-hop representations, which are then fused only at the prediction stage. This baseline is particularly important in our study because it strips decoupled MAG learning down to its simplest form: efficient independent propagation followed by shallow multimodal aggregation. As a result, MSGC serves as a direct probe of the modal conflict issue discussed in the introduction and appendix empirical analysis.

MGDN [17] is a recent decoupled multimodal method that leverages graph diffusion to produce efficient multimodal representations. Compared with simpler decoupled baselines such as SIGN or MSGC, MGDN introduces a stronger multimodal design while retaining the core efficiency advantage of precomputed propagation. We include MGDN as an especially relevant baseline because it is close to CAMPA along the efficiency axis, allowing us to test whether our gains truly come from aligned propagation and aggregation rather than from decoupling alone.

F Evaluation Protocols

To ensure a fair comparison across all methods, we evaluate every model under the same dataset split, graph topology, and modality inputs for each dataset-task pair. Unless otherwise specified, larger values indicate better performance.

Node Classification. Node classification is the basic supervised graph task. Given a MAG, each method encodes node v into a low-dimensional representation \mathbf{z}_v , which is then fed into a projection head and a softmax classifier. Optimization is performed by minimizing the cross-entropy loss on the labeled training nodes:

$$\mathcal{L}_{\text{nc}} = - \sum_{v \in \mathcal{V}_{\text{tr}}} \sum_{c=1}^C y_{v,c} \log \hat{y}_{v,c}, \quad (35)$$

where C is the number of classes, $y_{v,c}$ is the one-hot ground-truth label, and $\hat{y}_{v,c}$ is the predicted probability. We report Accuracy and F1-score on the test split.

Node Clustering. Node clustering evaluates the quality of learned node embeddings in an unsupervised setting. For each method, we first extract the final node representations and then apply the same clustering backend to produce semantic partitions. Following standard graph clustering evaluation, we report ACC, NMI, and ARI. Among them, NMI measures the mutual dependence between predicted clusters C and ground-truth labels Y :

$$\text{NMI}(Y, C) = \frac{2I(Y, C)}{H(Y) + H(C)}, \quad (36)$$

where $I(\cdot, \cdot)$ and $H(\cdot)$ denote mutual information and entropy, respectively. ARI evaluates clustering consistency from the perspective of sample pairs:

$$\text{ARI} = \frac{\sum_{ij} \binom{n_{ij}}{2} - \left[\sum_i \binom{a_i}{2} \sum_j \binom{b_j}{2} \right] / \binom{n}{2}}{\frac{1}{2} \left[\sum_i \binom{a_i}{2} + \sum_j \binom{b_j}{2} \right] - \left[\sum_i \binom{a_i}{2} \sum_j \binom{b_j}{2} \right] / \binom{n}{2}}, \quad (37)$$

where n_{ij} denotes the overlap between ground-truth cluster i and predicted cluster j .

Link Prediction. Link prediction evaluates whether the learned representations can identify missing or potential edges. For each query edge, the model computes scores for candidate node pairs and ranks positive edges above negative samples. We report ranking-based metrics including MRR, Hits@3, and Hits@10. Specifically, MRR is defined as

$$\text{MRR} = \frac{1}{|\mathcal{Q}|} \sum_{q \in \mathcal{Q}} \frac{1}{\text{rank}_q}, \quad (38)$$

where rank_q is the rank position of the first positive target for query q . Hits@K measures the fraction of queries whose positive target is ranked within the top- K candidates:

$$\text{Hits@K} = \frac{1}{|\mathcal{Q}|} \sum_{q \in \mathcal{Q}} \mathbb{I}(\text{rank}_q \leq K). \quad (39)$$

Modality Retrieval. Modality retrieval evaluates whether graph-aware representations improve bidirectional cross-modal search in a shared latent space. Given a source query from one modality, the model ranks candidates from the other modality by similarity. We report T2I-MRR and I2T-MRR, following the same ranking definition as MRR in link prediction.

Modality Matching. Modality matching measures whether paired textual and visual contents remain semantically consistent after graph-aware representation learning. We follow the CLIP-based evaluation protocol [26] and report the average CLIP-score on matched text-image pairs.

Modality Alignment. Modality alignment evaluates global semantic agreement between the textual and visual representations learned on the graph. Following the same CLIP-based protocol [26], we report the average alignment score between the two modalities. This task is particularly relevant to CAMPA because it directly reflects whether stage-wise alignment reduces cross-modal discrepancy in MAG learning.

G2Image. G2Image focuses on synthesizing images conditioned on graph-aware multimodal context, requiring the generated results to remain consistent with both the textual description and the graph structure. Following graph-conditioned generation protocols [38, 18], we evaluate the generated images with CLIP-Score and DINOv2-Score. Specifically, CLIP-Score measures cross-modal semantic consistency:

$$\text{CLIP-Score}(I, T) = \max(100 \cdot \cos(E_I(I), E_T(T)), 0), \quad (40)$$

where E_T and E_I denote the pre-trained CLIP text and image encoders [26]. DINOv2-Score evaluates visual fidelity and structural consistency against the reference image:

$$\text{DINOv2-Score}(I_{\text{gen}}, I_{\text{ref}}) = \cos(\text{DINO}(I_{\text{gen}}), \text{DINO}(I_{\text{ref}})), \quad (41)$$

where $\text{DINO}(\cdot)$ denotes the DINOv2 encoder [25]. Together, these two metrics reflect semantic faithfulness and perceptual consistency of graph-conditioned generation.

Repeated Runs and Reporting. When a task involves stochastic optimization, negative sampling, or clustering initialization, we repeat the evaluation under multiple random seeds and report the mean performance. The variability terms reported in tables are standard deviations computed over these repeated runs. All compared methods are evaluated with the same protocol on each dataset so that the reported differences can be attributed to the model design rather than to inconsistencies in splits, metrics, or evaluation backends.

G Experimental Settings

Shared Inputs and Preprocessing. All compared methods are evaluated on the same graph topology, train-validation-test split, and node-aligned multimodal contents for each dataset. The raw inputs consist of the graph structure together with textual and visual contents associated with each node. Before graph learning, the text and image contents are encoded by the same frozen pre-trained vision-language encoder, instantiated as Qwen2-VL-7B-Instruct [32], and the resulting embeddings are used as the initial modality features for all methods. If a baseline requires a task-specific hidden dimension, we apply the corresponding trainable projection only after this shared feature extraction stage, so that the fairness of the input protocol is preserved.

Algorithm Hyperparameters. For CAMPA, the propagation depth K is searched within $[2, 3, 4, 5]$. The hidden dimension is tuned over $[128, 256, 512]$. The number of multi-head attention heads is searched within $[2, 4, 8]$. The propagation coefficients are selected from $\alpha \in \{0.4, 0.5, 0.6\}$ and $\beta \in \{0.2, 0.3, 0.4\}$, while γ is determined by the constraint $\alpha + \beta + \gamma = 1$. The dropout rate is tuned in $[0.3, 0.4, 0.5]$. For baseline methods, we adopt the hyperparameter configurations reported in their original papers whenever available. For unspecified settings, we perform automated hyperparameter optimization using the Optuna framework.

Task Hyperparameters. For Node Classification and Node Clustering, the learning rate is searched within $[1 \times 10^{-5}, 5 \times 10^{-5}, 1 \times 10^{-4}, 1 \times 10^{-3}, 5 \times 10^{-3}]$, and the weight decay is tuned within $[1 \times 10^{-5}, 1 \times 10^{-4}]$. We fix the batch size to 512, the number of sampled neighbors to 25, and train the models for up to 300 epochs with an early-stop patience of 40. For Link Prediction, we set a fixed learning rate of 1×10^{-3} , batch size of 1024, and weight decay of 1×10^{-5} . The number of sampled neighbors is set to 15, the model is trained for up to 100 epochs, and early-stop patience is set to 20. For Modality Retrieval, Modality Matching, and Modality Alignment, we adopt task-specific downstream contrastive models and objectives with a temperature scaling factor $\tau = 0.1$. The models are trained for up to 500 epochs with a learning rate of 1×10^{-3} , batch size of 256, and early-stop patience of 50. For the G2Image [18] task, we adopt Stable Diffusion v1.5 as the image generation backbone. The model is trained with a learning rate of 1×10^{-4} , batch size of 16, and 10 training epochs. The input image resolution is set to 256, and graph-aware conditioning is injected with a cross-attention frequency of 2. We use 4 semantic neighbors for graph-conditioned generation. The optimization is performed with AdamW ($\beta_1 = 0.9$, $\beta_2 = 0.999$), weight decay of 0.01, and maximum gradient norm of 1.0. A constant learning-rate scheduler with 500 warmup steps is used. During inference, 50 denoising steps are adopted.

Experimental Environment. Experiments are conducted on a workstation equipped with an Intel(R) Xeon(R) Platinum 8470Q processor and an NVIDIA RTX PRO 6000 Blackwell Server Edition GPU with 96GB of VRAM, supported by 220GB of system RAM. The computational environment utilizes CUDA 13.1, while software implementations are developed using Python 3.10.18 and PyTorch 2.8.0.

H Additional Benchmark Results

This appendix provides additional benchmark results beyond the representative slices reported in the main text. Table 5 supplements the graph-centric evaluation with additional node classification and node clustering results, Table 6 further reports link prediction and G2Image results on representative dataset-task pairs, and Table 7 collects additional retrieval, matching, and alignment results. Taken together, these tables provide a broader empirical view of CAMPA across graph-centric and modality-centric settings.

Table 5: Additional graph-centric results on representative datasets.

Tasks		Node Classification				Node Clustering			
Methods	RedditS		Movies		Ele-fashion		RedditS		
	Acc	F1	Acc	F1	NMI	ARI	NMI	ARI	
GAT	94.21 \pm 0.13	90.23 \pm 0.13	53.98 \pm 0.24	43.57 \pm 0.24	35.45 \pm 0.30	17.04 \pm 0.30	37.40 \pm 0.30	17.78 \pm 0.30	
MMGCN	91.98 \pm 0.13	85.36 \pm 0.13	58.36 \pm 0.25	47.31 \pm 0.25	39.84 \pm 0.31	38.31 \pm 0.31	57.66 \pm 0.25	39.62 \pm 0.31	
MGAT	93.71 \pm 0.14	84.50 \pm 0.14	58.34 \pm 0.25	47.77 \pm 0.25	40.21 \pm 0.25	42.85 \pm 0.25	64.19 \pm 0.20	35.32 \pm 0.32	
DMGC	91.95 \pm 0.13	84.23 \pm 0.13	57.41 \pm 0.24	44.11 \pm 0.24	71.68 \pm 0.19	65.56 \pm 0.19	76.34 \pm 0.19	65.38 \pm 0.19	
DGF	94.88 \pm 0.13	87.13 \pm 0.13	59.51 \pm 0.24	50.33 \pm 0.24	75.02 \pm 0.19	64.90 \pm 0.19	78.40 \pm 0.19	66.99 \pm 0.19	
MIG-GT	95.31 \pm 0.09	88.61 \pm 0.14	59.01 \pm 0.25	46.12 \pm 0.25	59.77 \pm 0.25	48.51 \pm 0.25	62.13 \pm 0.20	51.30 \pm 0.25	
LGMRec	96.51 \pm 0.08	92.47 \pm 0.12	58.01 \pm 0.22	45.15 \pm 0.22	75.52 \pm 0.17	64.89 \pm 0.17	78.17 \pm 0.17	66.54 \pm 0.17	
UniGraph2	93.84 \pm 0.12	89.71 \pm 0.12	55.02 \pm 0.23	43.19 \pm 0.23	76.01 \pm 0.18	64.89 \pm 0.18	77.93 \pm 0.18	67.02 \pm 0.18	
CAMPA	96.76 \pm 0.08	92.51 \pm 0.11	61.04 \pm 0.16	53.33 \pm 0.20	76.50 \pm 0.16	67.33 \pm 0.16	81.03 \pm 0.11	71.03 \pm 0.16	

Table 6: Additional link prediction and G2Image results on representative dataset-task pairs.

Tasks		Link Prediction				G2Image			
Methods	Ele-fashion		Bili_music		Bili_music		RedditS		
	MRR	Hits@3	MRR	Hits@3	CLIP	DINOv2	CLIP	DINOv2	
GAT	65.23 \pm 0.19	75.63 \pm 0.19	53.77 \pm 0.24	66.50 \pm 0.19	49.42 \pm 0.24	21.00 \pm 0.30	63.04 \pm 0.19	19.86 \pm 0.30	
MMGCN	59.76 \pm 0.25	70.81 \pm 0.20	46.27 \pm 0.25	59.96 \pm 0.25	49.33 \pm 0.25	16.37 \pm 0.31	63.53 \pm 0.20	21.14 \pm 0.31	
MGAT	64.12 \pm 0.20	75.35 \pm 0.20	48.90 \pm 0.25	62.11 \pm 0.20	49.56 \pm 0.25	19.36 \pm 0.32	63.76 \pm 0.20	21.24 \pm 0.32	
DMGC	67.21 \pm 0.19	77.62 \pm 0.19	49.69 \pm 0.24	63.43 \pm 0.19	49.62 \pm 0.24	22.23 \pm 0.30	62.28 \pm 0.19	19.55 \pm 0.30	
DGF	64.14 \pm 0.19	73.54 \pm 0.19	46.48 \pm 0.24	57.92 \pm 0.24	47.35 \pm 0.24	18.36 \pm 0.30	62.63 \pm 0.19	19.12 \pm 0.30	
MIG-GT	63.22 \pm 0.20	72.51 \pm 0.20	47.62 \pm 0.25	61.21 \pm 0.20	52.58 \pm 0.25	25.49 \pm 0.32	63.39 \pm 0.20	20.82 \pm 0.32	
LGMRec	71.37 \pm 0.17	80.80 \pm 0.12	49.19 \pm 0.22	62.30 \pm 0.17	52.83 \pm 0.22	21.34 \pm 0.27	63.55 \pm 0.17	20.44 \pm 0.27	
UniGraph2	67.14 \pm 0.18	75.81 \pm 0.18	48.94 \pm 0.23	61.94 \pm 0.18	49.73 \pm 0.20	21.96 \pm 0.16	62.56 \pm 0.21	19.33 \pm 0.14	
CAMPA	74.74 \pm 0.16	85.20 \pm 0.11	60.89 \pm 0.16	78.62 \pm 0.16	53.16 \pm 0.20	23.24 \pm 0.26	64.27 \pm 0.16	21.60 \pm 0.26	

Table 7: Additional retrieval, matching, and alignment results on representative dataset-task pairs.

Tasks		Modality Retrieval		Modality Matching			Modality Alignment		
Methods	Bili_music		Ele-fashion	Bili_music	RedditS	Ele-fashion	Bili_music	RedditS	
	T2I	I2T	Score	Score	Score	Score	Score	Score	
GAT	98.55 \pm 0.09	98.47 \pm 0.09	99.38 \pm 0.06	99.41 \pm 0.06	97.65 \pm 0.09	99.58 \pm 0.06	98.33 \pm 0.09	97.19 \pm 0.09	
MMGCN	21.83 \pm 0.31	22.24 \pm 0.31	94.50 \pm 0.13	92.87 \pm 0.13	95.91 \pm 0.09	95.36 \pm 0.09	80.57 \pm 0.20	69.18 \pm 0.20	
MGAT	26.73 \pm 0.32	26.16 \pm 0.32	99.55 \pm 0.06	99.94 \pm 0.06	97.41 \pm 0.09	92.00 \pm 0.14	33.06 \pm 0.30	42.86 \pm 0.25	
DMGC	21.23 \pm 0.30	21.05 \pm 0.30	90.98 \pm 0.13	78.30 \pm 0.20	39.32 \pm 0.30	90.52 \pm 0.13	19.99 \pm 0.30	42.40 \pm 0.24	
DGF	95.92 \pm 0.09	96.13 \pm 0.09	99.74 \pm 0.06	99.65 \pm 0.06	99.90 \pm 0.06	95.15 \pm 0.09	60.61 \pm 0.19	84.51 \pm 0.13	
MIG-GT	23.17 \pm 0.32	22.34 \pm 0.32	98.95 \pm 0.09	86.41 \pm 0.13	90.21 \pm 0.14	94.93 \pm 0.14	40.83 \pm 0.25	79.57 \pm 0.20	
LGMRec	99.93 \pm 0.05	99.82 \pm 0.05	99.80 \pm 0.05	99.58 \pm 0.05	99.94 \pm 0.05	99.75 \pm 0.05	99.10 \pm 0.05	99.86 \pm 0.05	
UniGraph2	96.43 \pm 0.12	96.51 \pm 0.13	98.33 \pm 0.09	99.10 \pm 0.18	98.81 \pm 0.15	98.51 \pm 0.10	84.52 \pm 0.11	93.37 \pm 0.08	
CAMPA	99.34 \pm 0.05	98.72 \pm 0.08	99.33 \pm 0.05	99.23 \pm 0.05	99.37 \pm 0.05	99.92 \pm 0.05	87.36 \pm 0.08	96.05 \pm 0.08	

I Limitations and Broader Impacts

Limitations. Our framework currently focuses on MAGs with textual and visual modalities, and extending the same design to richer modality combinations may require additional adaptation. Moreover, CAMPA relies on frozen pretrained encoders to construct the initial node features, so the final performance is still partially constrained by the quality and domain fit of the upstream encoder. While our theoretical analysis supports the stability of aligned propagation and aggregation, more refined questions such as generalization under stronger distribution shifts remain open.

Broader Impacts. CAMPA provides a scalable framework for improving multimodal graph learning under decoupled propagation and aggregation. By enhancing cross-modal consistency while preserving efficiency, it may benefit recommendation, social content understanding, retrieval, and graph-conditioned generation in practical applications. At the same time, stronger multimodal graph models may inherit or amplify biases, privacy risks, or unintended profiling effects from the underlying graph data and pretrained encoders, especially in recommendation and social-content applications. When used in graph-conditioned generation, the framework should therefore be deployed with appropriate dataset governance, monitoring, and task-specific safeguards.

NeurIPS Paper Checklist

1. Claims

Question: Do the main claims made in the abstract and introduction accurately reflect the paper’s contributions and scope?

Answer: [Yes]

Justification: The abstract and introduction state the central claim that CAMPA addresses modal conflict in decoupled MAG learning through aligned propagation and aggregation. These claims are supported by the method, theory, and experimental sections, including Secs. 1–4.

Guidelines:

- The answer [N/A] means that the abstract and introduction do not include the claims made in the paper.
- The abstract and/or introduction should clearly state the claims made, including the contributions made in the paper and important assumptions and limitations. A [No] or [N/A] answer to this question will not be perceived well by the reviewers.
- The claims made should match theoretical and experimental results, and reflect how much the results can be expected to generalize to other settings.
- It is fine to include aspirational goals as motivation as long as it is clear that these goals are not attained by the paper.

2. Limitations

Question: Does the paper discuss the limitations of the work performed by the authors?

Answer: [Yes]

Justification: The paper includes a dedicated limitations discussion in Appendix I, covering the current modality scope, dependence on frozen pretrained encoders, and the scope of the theory.

Guidelines:

- The answer [N/A] means that the paper has no limitation while the answer [No] means that the paper has limitations, but those are not discussed in the paper.
- The authors are encouraged to create a separate “Limitations” section in their paper.
- The paper should point out any strong assumptions and how robust the results are to violations of these assumptions (e.g., independence assumptions, noiseless settings, model well-specification, asymptotic approximations only holding locally). The authors should reflect on how these assumptions might be violated in practice and what the implications would be.
- The authors should reflect on the scope of the claims made, e.g., if the approach was only tested on a few datasets or with a few runs. In general, empirical results often depend on implicit assumptions, which should be articulated.
- The authors should reflect on the factors that influence the performance of the approach. For example, a facial recognition algorithm may perform poorly when image resolution is low or images are taken in low lighting. Or a speech-to-text system might not be used reliably to provide closed captions for online lectures because it fails to handle technical jargon.
- The authors should discuss the computational efficiency of the proposed algorithms and how they scale with dataset size.
- If applicable, the authors should discuss possible limitations of their approach to address problems of privacy and fairness.
- While the authors might fear that complete honesty about limitations might be used by reviewers as grounds for rejection, a worse outcome might be that reviewers discover limitations that aren’t acknowledged in the paper. The authors should use their best judgment and recognize that individual actions in favor of transparency play an important role in developing norms that preserve the integrity of the community. Reviewers will be specifically instructed to not penalize honesty concerning limitations.

3. Theory assumptions and proofs

Question: For each theoretical result, does the paper provide the full set of assumptions and a complete (and correct) proof?

Answer: [Yes]

Justification: The main text states the theoretical results and their assumptions in Sec. 3.3, and the complete proofs are provided in Appendix B.

Guidelines:

- The answer [N/A] means that the paper does not include theoretical results.
- All the theorems, formulas, and proofs in the paper should be numbered and cross-referenced.
- All assumptions should be clearly stated or referenced in the statement of any theorems.
- The proofs can either appear in the main paper or the supplemental material, but if they appear in the supplemental material, the authors are encouraged to provide a short proof sketch to provide intuition.
- Inversely, any informal proof provided in the core of the paper should be complemented by formal proofs provided in appendix or supplemental material.
- Theorems and Lemmas that the proof relies upon should be properly referenced.

4. Experimental result reproducibility

Question: Does the paper fully disclose all the information needed to reproduce the main experimental results of the paper to the extent that it affects the main claims and/or conclusions of the paper (regardless of whether the code and data are provided or not)?

Answer: [Yes]

Justification: The paper specifies the datasets, baselines, evaluation protocols, algorithm pipeline, and experimental settings in Sec. 4 and Appendices D–G, which together disclose the information needed to reproduce the reported setup.

Guidelines:

- The answer [N/A] means that the paper does not include experiments.
- If the paper includes experiments, a [No] answer to this question will not be perceived well by the reviewers: Making the paper reproducible is important, regardless of whether the code and data are provided or not.
- If the contribution is a dataset and/or model, the authors should describe the steps taken to make their results reproducible or verifiable.
- Depending on the contribution, reproducibility can be accomplished in various ways. For example, if the contribution is a novel architecture, describing the architecture fully might suffice, or if the contribution is a specific model and empirical evaluation, it may be necessary to either make it possible for others to replicate the model with the same dataset, or provide access to the model. In general, releasing code and data is often one good way to accomplish this, but reproducibility can also be provided via detailed instructions for how to replicate the results, access to a hosted model (e.g., in the case of a large language model), releasing of a model checkpoint, or other means that are appropriate to the research performed.
- While NeurIPS does not require releasing code, the conference does require all submissions to provide some reasonable avenue for reproducibility, which may depend on the nature of the contribution. For example
 - (a) If the contribution is primarily a new algorithm, the paper should make it clear how to reproduce that algorithm.
 - (b) If the contribution is primarily a new model architecture, the paper should describe the architecture clearly and fully.
 - (c) If the contribution is a new model (e.g., a large language model), then there should either be a way to access this model for reproducing the results or a way to reproduce the model (e.g., with an open-source dataset or instructions for how to construct the dataset).
 - (d) We recognize that reproducibility may be tricky in some cases, in which case authors are welcome to describe the particular way they provide for reproducibility. In the case of closed-source models, it may be that access to the model is limited in

some way (e.g., to registered users), but it should be possible for other researchers to have some path to reproducing or verifying the results.

5. Open access to data and code

Question: Does the paper provide open access to the data and code, with sufficient instructions to faithfully reproduce the main experimental results, as described in supplemental material?

Answer: [Yes]

Justification: All datasets are publicly available. The code and instructions to reproduce the results are included in the supplemental material.

Guidelines:

- The answer [N/A] means that paper does not include experiments requiring code.
- Please see the NeurIPS code and data submission guidelines (<https://neurips.cc/public/guides/CodeSubmissionPolicy>) for more details.
- While we encourage the release of code and data, we understand that this might not be possible, so [No] is an acceptable answer. Papers cannot be rejected simply for not including code, unless this is central to the contribution (e.g., for a new open-source benchmark).
- The instructions should contain the exact command and environment needed to run to reproduce the results. See the NeurIPS code and data submission guidelines (<https://neurips.cc/public/guides/CodeSubmissionPolicy>) for more details.
- The authors should provide instructions on data access and preparation, including how to access the raw data, preprocessed data, intermediate data, and generated data, etc.
- The authors should provide scripts to reproduce all experimental results for the new proposed method and baselines. If only a subset of experiments are reproducible, they should state which ones are omitted from the script and why.
- At submission time, to preserve anonymity, the authors should release anonymized versions (if applicable).
- Providing as much information as possible in supplemental material (appended to the paper) is recommended, but including URLs to data and code is permitted.

6. Experimental setting/details

Question: Does the paper specify all the training and test details (e.g., data splits, hyperparameters, how they were chosen, type of optimizer) necessary to understand the results?

Answer: [Yes]

Justification: The experimental setting is summarized in Sec. 4, while the full details of datasets, metrics, hyperparameters, optimization strategy, and environment are provided in Appendices D, F, and G.

Guidelines:

- The answer [N/A] means that the paper does not include experiments.
- The experimental setting should be presented in the core of the paper to a level of detail that is necessary to appreciate the results and make sense of them.
- The full details can be provided either with the code, in appendix, or as supplemental material.

7. Experiment statistical significance

Question: Does the paper report error bars suitably and correctly defined or other appropriate information about the statistical significance of the experiments?

Answer: [Yes]

Justification: The experimental tables report mean performance together with standard deviations over repeated runs, and Appendix F explicitly states that the variability terms are standard deviations computed across multiple random seeds.

Guidelines:

- The answer [N/A] means that the paper does not include experiments.

- The authors should answer [Yes] if the results are accompanied by error bars, confidence intervals, or statistical significance tests, at least for the experiments that support the main claims of the paper.
- The factors of variability that the error bars are capturing should be clearly stated (for example, train/test split, initialization, random drawing of some parameter, or overall run with given experimental conditions).
- The method for calculating the error bars should be explained (closed form formula, call to a library function, bootstrap, etc.)
- The assumptions made should be given (e.g., Normally distributed errors).
- It should be clear whether the error bar is the standard deviation or the standard error of the mean.
- It is OK to report 1-sigma error bars, but one should state it. The authors should preferably report a 2-sigma error bar than state that they have a 96% CI, if the hypothesis of Normality of errors is not verified.
- For asymmetric distributions, the authors should be careful not to show in tables or figures symmetric error bars that would yield results that are out of range (e.g., negative error rates).
- If error bars are reported in tables or plots, the authors should explain in the text how they were calculated and reference the corresponding figures or tables in the text.

8. Experiments compute resources

Question: For each experiment, does the paper provide sufficient information on the computer resources (type of compute workers, memory, time of execution) needed to reproduce the experiments?

Answer: [Yes]

Justification: We provide efficiency analysis in Sec. 4.4 and report the hardware and software environment in Appendix G. This includes the GPU type, memory, and system configuration used in our experiments.

Guidelines:

- The answer [N/A] means that the paper does not include experiments.
- The paper should indicate the type of compute workers CPU or GPU, internal cluster, or cloud provider, including relevant memory and storage.
- The paper should provide the amount of compute required for each of the individual experimental runs as well as estimate the total compute.
- The paper should disclose whether the full research project required more compute than the experiments reported in the paper (e.g., preliminary or failed experiments that didn't make it into the paper).

9. Code of ethics

Question: Does the research conducted in the paper conform, in every respect, with the NeurIPS Code of Ethics <https://neurips.cc/public/EthicsGuidelines>?

Answer: [Yes]

Justification: To the best of our knowledge, the research follows the NeurIPS Code of Ethics. The work is based on public datasets, standard benchmarking practice, and does not involve deceptive experimental procedures or human subject studies.

Guidelines:

- The answer [N/A] means that the authors have not reviewed the NeurIPS Code of Ethics.
- If the authors answer [No], they should explain the special circumstances that require a deviation from the Code of Ethics.
- The authors should make sure to preserve anonymity (e.g., if there is a special consideration due to laws or regulations in their jurisdiction).

10. Broader impacts

Question: Does the paper discuss both potential positive societal impacts and negative societal impacts of the work performed?

Answer: [Yes]

Justification: The paper includes a dedicated broader-impact discussion in Appendix I, covering both the positive value of efficient MAG learning and potential risks related to multimodal recommendation, profiling, and graph-conditioned generation.

Guidelines:

- The answer [N/A] means that there is no societal impact of the work performed.
- If the authors answer [N/A] or [No], they should explain why their work has no societal impact or why the paper does not address societal impact.
- Examples of negative societal impacts include potential malicious or unintended uses (e.g., disinformation, generating fake profiles, surveillance), fairness considerations (e.g., deployment of technologies that could make decisions that unfairly impact specific groups), privacy considerations, and security considerations.
- The conference expects that many papers will be foundational research and not tied to particular applications, let alone deployments. However, if there is a direct path to any negative applications, the authors should point it out. For example, it is legitimate to point out that an improvement in the quality of generative models could be used to generate Deepfakes for disinformation. On the other hand, it is not needed to point out that a generic algorithm for optimizing neural networks could enable people to train models that generate Deepfakes faster.
- The authors should consider possible harms that could arise when the technology is being used as intended and functioning correctly, harms that could arise when the technology is being used as intended but gives incorrect results, and harms following from (intentional or unintentional) misuse of the technology.
- If there are negative societal impacts, the authors could also discuss possible mitigation strategies (e.g., gated release of models, providing defenses in addition to attacks, mechanisms for monitoring misuse, mechanisms to monitor how a system learns from feedback over time, improving the efficiency and accessibility of ML).

11. Safeguards

Question: Does the paper describe safeguards that have been put in place for responsible release of data or models that have a high risk for misuse (e.g., pre-trained language models, image generators, or scraped datasets)?

Answer: [N/A]

Justification: The current submission does not release a new high-risk model, image generator, or scraped dataset artifact. The paper studies existing datasets and standard pretrained backbones within a research setting.

Guidelines:

- The answer [N/A] means that the paper poses no such risks.
- Released models that have a high risk for misuse or dual-use should be released with necessary safeguards to allow for controlled use of the model, for example by requiring that users adhere to usage guidelines or restrictions to access the model or implementing safety filters.
- Datasets that have been scraped from the Internet could pose safety risks. The authors should describe how they avoided releasing unsafe images.
- We recognize that providing effective safeguards is challenging, and many papers do not require this, but we encourage authors to take this into account and make a best faith effort.

12. Licenses for existing assets

Question: Are the creators or original owners of assets (e.g., code, data, models), used in the paper, properly credited and are the license and terms of use explicitly mentioned and properly respected?

Answer: [Yes]

Justification: We cite all datasets and code used and ensure compliance with their respective licenses.

Guidelines:

- The answer [N/A] means that the paper does not use existing assets.
- The authors should cite the original paper that produced the code package or dataset.
- The authors should state which version of the asset is used and, if possible, include a URL.
- The name of the license (e.g., CC-BY 4.0) should be included for each asset.
- For scraped data from a particular source (e.g., website), the copyright and terms of service of that source should be provided.
- If assets are released, the license, copyright information, and terms of use in the package should be provided. For popular datasets, paperswithcode.com/datasets has curated licenses for some datasets. Their licensing guide can help determine the license of a dataset.
- For existing datasets that are re-packaged, both the original license and the license of the derived asset (if it has changed) should be provided.
- If this information is not available online, the authors are encouraged to reach out to the asset's creators.

13. **New assets**

Question: Are new assets introduced in the paper well documented and is the documentation provided alongside the assets?

Answer: [N/A]

Justification: The current submission does not release a new dataset, benchmark package, codebase, or model checkpoint as an external asset.

Guidelines:

- The answer [N/A] means that the paper does not release new assets.
- Researchers should communicate the details of the dataset/code/model as part of their submissions via structured templates. This includes details about training, license, limitations, etc.
- The paper should discuss whether and how consent was obtained from people whose asset is used.
- At submission time, remember to anonymize your assets (if applicable). You can either create an anonymized URL or include an anonymized zip file.

14. **Crowdsourcing and research with human subjects**

Question: For crowdsourcing experiments and research with human subjects, does the paper include the full text of instructions given to participants and screenshots, if applicable, as well as details about compensation (if any)?

Answer: [N/A]

Justification: The paper does not involve crowdsourcing or research with human subjects.

Guidelines:

- The answer [N/A] means that the paper does not involve crowdsourcing nor research with human subjects.
- Including this information in the supplemental material is fine, but if the main contribution of the paper involves human subjects, then as much detail as possible should be included in the main paper.
- According to the NeurIPS Code of Ethics, workers involved in data collection, curation, or other labor should be paid at least the minimum wage in the country of the data collector.

15. **Institutional review board (IRB) approvals or equivalent for research with human subjects**

Question: Does the paper describe potential risks incurred by study participants, whether such risks were disclosed to the subjects, and whether Institutional Review Board (IRB) approvals (or an equivalent approval/review based on the requirements of your country or institution) were obtained?

Answer: [N/A]

Justification: The paper does not involve human subject research and therefore does not require IRB approval or related disclosures.

Guidelines:

- The answer [N/A] means that the paper does not involve crowdsourcing nor research with human subjects.
- Depending on the country in which research is conducted, IRB approval (or equivalent) may be required for any human subjects research. If you obtained IRB approval, you should clearly state this in the paper.
- We recognize that the procedures for this may vary significantly between institutions and locations, and we expect authors to adhere to the NeurIPS Code of Ethics and the guidelines for their institution.
- For initial submissions, do not include any information that would break anonymity (if applicable), such as the institution conducting the review.

16. **Declaration of LLM usage**

Question: Does the paper describe the usage of LLMs if it is an important, original, or non-standard component of the core methods in this research? Note that if the LLM is used only for writing, editing, or formatting purposes and does *not* impact the core methodology, scientific rigor, or originality of the research, declaration is not required.

Answer: [N/A]

Justification: The core methodological contribution of the paper does not depend on an LLM as an important, original, or non-standard component. The use of a pretrained vision-language encoder is part of the experimental input protocol rather than the core methodological novelty.

Guidelines:

- The answer [N/A] means that the core method development in this research does not involve LLMs as any important, original, or non-standard components.
- Please refer to our LLM policy in the NeurIPS handbook for what should or should not be described.